Fisheries and Oceans Canada | Pêches et Océans Canada
Ecosystems and Oceans Science | Sciences des écosystèmes et des océans

Canadian Science Advisory Secretariat (CSAS)

Research Document 2017/034

Québec Region

Chemical and Biological Oceanographic Conditions in the Estuary and Gulf of St. Lawrence during 2015

L. Devine, M. Scarratt, S. Plourde, P. S. Galbraith, S. Michaud, and C. Lehoux

Fisheries and Oceans Canada
Institut Maurice-Lamontagne
850 route de la Mer, P.O. Box 1000
Mont-Joli, QC, G5H 3Z4

May 2017

Canada

Foreword

This series documents the scientific basis for the evaluation of aquatic resources and ecosystems in Canada. As such, it addresses the issues of the day in the time frames required and the documents it contains are not intended as definitive statements on the subjects addressed but rather as progress reports on ongoing investigations.

Research documents are produced in the official language in which they are provided to the Secretariat.

Published by:

Fisheries and Oceans Canada
Canadian Science Advisory Secretariat
200 Kent Street
Ottawa ON K1A 0E6

http://www.dfo-mpo.gc.ca/csas-sccs/
csas-sccs@dfo-mpo.gc.ca

© Her Majesty the Queen in Right of Canada, 2017
ISSN 1919-5044

Correct citation for this publication:

Devine, L., Scarratt, M., Plourde, S., Galbraith, P.S., Michaud, S., and Lehoux, C. 2017. Chemical and Biological Oceanographic Conditions in the Estuary and Gulf of St. Lawrence during 2015. DFO Can. Sci. Advis. Sec. Res. Doc. 2017/034. v + 48 pp.

TABLE OF CONTENTS

ABSTRACT IV

RÉSUMÉ V

INTRODUCTION 1

METHODS 1

RESULTS 4

NUTRIENTS AND PHYTOPLANKTON 4

High-frequency monitoring sites 4

Sections and late winter helicopter survey 5

Remote sensing of ocean colour 6

ZOOPLANKTON 7

High-frequency monitoring sites 7

Gulf subregions 8

Copepod phenology 8

Scorecards 9

DISCUSSION 9

SUMMARY 13

ACKNOWLEDGEMENTS 14

REFERENCES 14

TABLES 17

FIGURES 18

ABSTRACT

An overview of chemical and biological oceanographic conditions in the Gulf of St. Lawrence (GSL) in 2015 is presented as part of the Atlantic Zone Monitoring Program (AZMP). AZMP data as well as data from regional monitoring programs are analyzed and presented in relation to long-term means in the context of a strong warming event that began in 2010. In 2015, sea-surface temperatures were near normal from May to November while deepwater temperatures reached an all-time high. Nitrate inventories in 2015 were near normal in the 0–50 m layer but strongly above normal in the deeper layer, the latter in association with high temperatures and salinities. Compared to the time series (1999–2010), the spring phytoplankton bloom began earlier, lasted longer, and had a greater magnitude in the NWGSL and NEGSL while the reverse was observed for the Magdalen Shallows and Cabot Strait. The shift away from a smaller-sized phytoplankton community at Rimouski station continued in 2015, with a second consecutive year of positive anomalies in the diatom/flagellate ratios, while increased relative abundances of the smaller-sized phytoplankton—dinoflagellates and ciliates—were observed at Shediac Valley. Zooplankton biomass was below normal throughout the GSL, with strong declines in the indices for *Calanus finmarchicus*, large calanoids, and cold-water copepods and strong increases for *Pseudocalanus* spp., small calanoids, warm-water copepods, and non-copepods. The overall high Gulf-wide temperatures (surface and deep layers) and salinities observed in 2015 likely led to the well-above-normal abundances of warm-water copepod species as well as the presence of specimens from the family Aetideidae, which appeared in the top 95% of the most abundant copepod taxa for the first time in 2014.

Les conditions océanographiques chimiques et biologiques dans l'estuaire et le golfe du Saint-Laurent en 2015

RÉSUMÉ

Un aperçu des conditions océanographiques chimiques et biologiques du golfe du Saint-Laurent (GSL) en 2015 est présenté dans le cadre du Programme de monitorage de la zone atlantique (PMZA). Les données du PMZA, ainsi que celles provenant de programmes de monitorage régionaux, sont analysées et présentées en fonction des moyennes à long terme dans le contexte d'un événement de réchauffement ayant commencé en 2010. En 2015, les températures de surface du GSL étaient presque normales de mai à novembre tandis que les températures des couches profondes atteignaient un niveau record de chaleur. Les concentrations de nitrates en 2015 étaient presque normales dans la couche de 0–50 m, mais fortement supérieures à la normale dans la couche plus profonde, ces dernières étant associées à des températures et des salinités élevées. Selon la moyenne à long terme (1999–2010), la prolifération printanière du phytoplancton en 2015 fut hâtive, plus longue et de plus grande ampleur au nord-ouest et au nord-est du GSL, tandis qu'aux Plateau madelinien et détroit de Cabot, une tendance inverse était observée. À la station Rimouski, la tendance au changement de structure de la communauté phytoplanctonique, de petites vers de plus grosses tailles s'est poursuivie en 2015, avec une seconde année consécutive d'anomalies positives des rapports diatomées / flagellés. Cependant, l'augmentation d'abondance relative des dinoflagellés et ciliés (petites tailles) a été observée à Shediac Valley. La biomasse de zooplancton était inférieure à la normale dans l'ensemble du GSL, avec de fortes baisses d'indices de *Calanus finmarchicus*, des grands calanoïdes et des copépodes d'eau froide et de fortes augmentations de *Pseudocalanus* spp., des petits calanoïdes, des copépodes d'eau chaude et des non-copépodes. Les températures élevées dans le golfe (couches de surface et profondes) et les fortes salinités des eaux profondes observées en 2015 expliquent probablement les abondances très supérieures à la normale de plusieurs espèces de copépodes d'eau chaude ainsi que de ceux appartenant à la famille des Aetideidae, ces derniers faisant maintenant partie de la liste des taxons représentant 95 % de l'abondance totale des copépodes dans la région.

INTRODUCTION

The Atlantic Zone Monitoring Program (AZMP) was implemented in 1998 (Therriault et al. 1998) with the aim of (1) increasing Fisheries and Oceans Canada's (DFO) capacity to understand, describe, and forecast the state of the marine ecosystem and (2) quantifying the changes in the ocean's physical, chemical, and biological properties and the predator–prey relationships of marine resources. AZMP provides data to support the sound development of ocean activities. A critical element in the observational program of AZMP is an annual assessment of the distribution and variability of nutrients and the plankton they support.

A description of the spatiotemporal distribution of nutrients (nitrate, silicate, phosphate), chlorophyll concentrations, and oxygen dissolved in seawater provides important information on water-mass movements and on the locations, timing, and magnitude of biological production cycles. A description of phytoplankton and zooplankton distribution provides important information on the organisms forming the base of the marine food web. An understanding of plankton production cycles is an essential part of an ecosystem approach to fisheries management.

The AZMP derives its information on the state of the marine ecosystem from data collected at a network of sampling locations (high-frequency monitoring sites, cross-shelf sections) in each DFO region (Québec, Gulf, Maritimes, Newfoundland; see Figure 1 for Québec region locations) sampled at a frequency of weekly to once annually. The sampling design provides basic information on the natural variability in physical, chemical, and biological properties of the Northwest Atlantic continental shelf: cross-shelf sections provide detailed geographic information but are limited in their seasonal coverage while critically placed high-frequency monitoring sites complement the geography-based sampling by providing more detailed information on temporal (seasonal) changes in ecosystem properties.

In this document, we review the chemical and biological oceanographic (lower trophic levels) conditions in the Gulf of St. Lawrence (GSL) in 2015. Overall, temperature conditions were somewhat warmer than normal, especially in August and September, following a delayed onset after cold winter conditions (above-normal surface mixed cold layer depth and above-normal sea-ice volume due to the coldest February since 1993; Galbraith et al. 2016). Deepwater temperatures have continued to increase as have the bottom areas covered by waters warmer than 6°C because of inward advection of warm water through Cabot Strait; both of these saw record-high values in 2015 (Galbraith et al. 2016). This report describes the 2015 production cycles and community composition of phytoplankton and zooplankton in this context.

METHODS

All sample collection and processing steps meet and often exceed the standards of the AZMP protocol (Mitchell et al. 2002). Field measurements included in this report were collected along seven sections during surveys done in June and October–November of each year and at two high-frequency monitoring sites (Fig. 1). Table 1 provides details about the 2015 sampling missions and Figure 2 gives the sampling effort at the high-frequency sampling sites. Rimouski station (RS; depth 320 m) has been sampled since 1991 as part of a research project—about weekly throughout the summer, less frequently in early spring and late fall, and rarely in winter (except for physical variables during the March helicopter survey). It has been included in AZMP's annual review of environmental conditions since 2004 (AZMP 2006) to represent conditions in the St. Lawrence Estuary (SLE) and the northwest GSL. Since the beginning of the AZMP, Shediac Valley station (SV; depth 84 m) has represented conditions in the southern GSL

and SLE outflow. While the goal is to sample SV weekly, the frequency is closer to monthly and rarely during January–April because of its remoteness. Sampling at sections and high-frequency monitoring sites includes a CTD profile (temperature, salinity, fluorescence, dissolved oxygen, pH) as well as water sampling using Niskin bottles. Water from the Niskin bottles was collected for the analysis of dissolved oxygen (Winkler titrations), chlorophyll *a* (method of Welschmeyer 1994), nutrients, and phytoplankton identification. Finally, zooplankton were sampled with bottom-to-surface ring net tows (75 cm diameter, 200 µm mesh) for identification and biomass measurements.

Since 1996, a survey has been conducted of the winter surface mixed layer of the GSL in early to mid-March using a Canadian Coast Guard helicopter; surface nutrients (2 m) were added to the sampling protocol in 2001 (Galbraith 2006, Galbraith et al. 2006). This survey has added a considerable amount of data to the previously sparse winter sampling in the region. A total of 74 stations were sampled during the 3–12 March 2015 survey. The temperature and salinity of the 2015 mixed layer are described by Galbraith et al. (2016).

Near-surface phytoplankton biomass has been estimated from ocean colour data collected by the Sea-viewing Wide Field-of-view Sensor (SeaWiFS) satellite launched by NASA in late summer 1997, by the Moderate Resolution Imaging Spectroradiometer (MODIS) "Aqua" sensor launched by NASA in July 2002, and most recently by the Visible Infrared Imaging Radiometer Suite (VIIRS) satellite, which was launched in October 2011. In this report, VIIRS data from July to November 2015 and MODIS data from January 2008 until June 2015 are combined with SeaWiFS data from September 1997 until December 2007 to construct composite time series of surface chlorophyll *a* (chl *a*) in four GSL subregions (northwest and northeast GSL, Magdalen Shallows, Cabot Strait; see Fig. 3 for locations). The performance of the MODIS satellite to estimate chl *a* has been compared with that of SeaWiFS for some regions of the globe. Although differences in sensor design, orbit, and sampling between MODIS and SeaWiFS cause some differences in calculated chl *a* values (Gregg and Rousseaux 2014), the performance of both satellites is relatively good and comparable. The biases associated with the different satellites are overall not significantly greater than algorithm uncertainties, particularly in non-turbid waters (Zibordi et al. 2006, Arun Kumar et al. 2015). Recent studies comparing the all three sensors indicate that they provide consistent global ocean colour data records, with similar patterns and magnitudes and generally high cross-sensor fidelity (Wang et al. 2013, Barnes and Hu, 2016).

All selected subregions for the imagery data are located outside of the St. Lawrence River plume because data in regions influenced by this freshwater are unreliable due to turbidity and riverine input of terrestrially derived coloured matter. Composite satellite images were provided by BIO's remote sensing unit (Bedford Institute of Oceanography, DFO, Dartmouth, NS) in collaboration with NASA's GSFC (Goddard Space Flight Center). Basic statistics (mean, range, standard deviation) were extracted from two-week average composites with a 1.5 km spatial resolution for SeaWiFS and MODIS and from quarter-monthly (eight-day) composites for VIIRS.

A shifted Gaussian function of time model was used to describe characteristics of the spring phytoplankton bloom based on the combined satellite data (Zhai et al. 2011). Four different metrics were computed to describe the spring bloom characteristics: start date (day of year), cycle duration (days), magnitude (the integral of chl *a* concentration under the Gaussian curve), and amplitude (maximum chl *a*). In addition, the mean chlorophyll biomass during spring (March to May), summer (June to August), and fall (September to November) as well as its annual average (March to November) were computed. For each of these eight metrics, we computed normalized annual anomalies (see below) to evaluate evidence of temporal trends among the different statistical subregions.

Chlorophyll *a* and nutrient data collected along the AZMP sections and the high-frequency monitoring sites were integrated over various depth intervals (i.e., 0–100 m for chl *a*; 0–50 m and 50–150 m for nutrients) using trapezoidal numerical integration. The surface (0 m) data were actually the shallowest sampled values; data at the lower depths were taken as either (i) the interpolated value when sampling was below the lower integration limit or (ii) the closest deepwater sampled value when sampling was shallower than the lower integration limit. Integrated nitrate values from the helicopter survey were calculated using surface concentrations (2 m) × 50 m; it was assumed that nitrate concentrations are homogeneous in the winter mixed layer at that time of the year.

In this document, we give a detailed description of the seasonal patterns in zooplankton indices for RS and SV. In recent years, the number and type of zooplankton indices as well as the way they are reported have been rationalized with the aim of standardizing research documents among AZMP regions. We thus present total zooplankton biomass, total copepod abundance, and the relative contributions of the copepod species making up 95% of the identified taxa. In addition, we include *Pseudocalanus* spp. (RS only) and *Calanus finmarchicus* abundances and stage composition for the high-frequency monitoring sites. Because of its importance to the total zooplankton biomass in this region, a detailed description of *Calanus hyperboreus* has been added. We present the spring and fall total zooplankton biomass and total abundance of *C. finmarchicus*, *C. hyperboreus*, and *Pseudocalanus* spp. for three regions having distinct oceanographic regimes (Fig. 1) and corresponding more to the spatial scales addressed by AZMP in other regions:

(1) western GSL (wGSL): this region is generally deep (> 200 m) and cold in summer. It is strongly influenced by freshwater runoff from the St. Lawrence River and cold and dense waters from the Laurentian Channel;

(2) southern GSL (sGSL): this region is shallow (< 100 m) and much warmer in summer. It is under the influence of the Gaspé Current;

(3) eastern GSL (eGSL): this region, with deep channels and a relatively wide shelf (< 100 m), is characterized by higher surface salinity and is directly influenced by the intrusion of water from the Labrador and Newfoundland shelves.

Standardized anomalies of key chemical and biological indices were computed for the high-frequency monitoring sites, sections, and oceanographic regions. These anomalies are calculated as the difference between the variable's average for the season (i.e., chlorophyll and nutrient indices) or for the complete year (i.e., zooplankton indices) and the variable's average for the reference period (usually 1999–2010); this number is then divided by the reference period's standard deviation. Only actual measurements were used for these calculations, not modelled data. These anomalies thus represent observations in a compact ("scorecard") format, with positive anomalies depicted as shades of red on the scorecard, negatives as blues, and neutral as white. A standard set of indices representing anomalies of nutrient availability, phytoplankton biomass and bloom dynamics, and the abundance of dominant copepod species and groups (*C. finmarchicus*, *Pseudocalanus* spp., total copepods, and total non-copepods) are produced for each AZMP region (see DFO 2016). We also present several zooplankton indices that reflect either different functional groups with different roles in the ecosystem or groups of species indicative of cold- or warm-water intrusions and/or local temperature conditions specific to the GSL. These indices are for large calanoids (dominated by *Calanus* and *Metridia* species), small calanoids (dominated by more neritic species such as *Pseudocalanus* spp., *Acartia* spp., *Temora longicornis*, and *Centropages* spp.), cyclopoids (dominated by *Oithona* spp. and *Triconia* spp.; the latter is a poecilostomatoid that is included in this category because of its ecological characteristics), warm-water species (*Metridia lucens*, *Centropages* spp.,

Paracalanus spp., and *Clausocalanus* spp.), and cold/arctic species (*Calanus glacialis* and *Metridia longa*). It should be noted that these zooplankton anomalies were calculated using station depth rather than sampled depth in previous reports (e.g., Devine et al. 2015), thus numbers in the scorecard do not exactly match previous values even though anomaly patterns have not changed.

Changes in zooplankton phenology were described using *C. finmarchicus* as an indicator. We used the time series at RS because adequate sampling and stage identification started there more than 20 years ago (1994). From 1994 to 2004, *C. finmarchicus* copepodite stage abundance was determined using samples collected with 333 µm (CIV–CVI) and 73 µm (CI–III) mesh nets that were analyzed for seven years of the time series (see Plourde et al. 2009 for details). In other years before 2004 for which 73 µm samples were not analyzed, the abundance of CI–III in the 333 µm samples was adjusted based on a comparison done with an AZMP-like net (S. Plourde, DFO, Mont-Joli, Qc, unpublished data). The phenology of *C. finmarchicus* was described using the following steps: (1) stage abundance data (ind m^{-2}) were normalized (x/x_{max}) within each year for CI–III, CIV, CV, and CVI (male and female) and (2) relative stage proportions were smoothed using a Loess algorithm.

RESULTS

NUTRIENTS AND PHYTOPLANKTON

Distributions of the primary dissolved inorganic nutrients (nitrate, silicate, phosphate) included in AZMP's observational program strongly co-vary in space and time (Brickman and Petrie 2003). For this reason and because the availability of nitrogen is most often associated with phytoplankton growth limitation in coastal waters of the GSL, emphasis in this document is placed on variability in nitrate concentrations and inventories. In this document, we use the term "nitrate" to refer to nitrite+nitrate (NO_2^-+NO_3^-).

High-frequency monitoring sites

The Rimouski and Shediac Valley stations typically exhibit a biologically mediated reduction in surface nitrate inventories in spring/summer, a minimum during summer, and a subsequent increase during fall/winter (Fig. 4); the patterns in 2015 were very similar to the 1999–2010 means. The nutrient draw-down occurs later at RS compared to SV, reflecting the later spring bloom in the SLE (May–July in 2015) compared to SV (April). The early spring bloom at SV was not captured by the 2015 sampling; nevertheless, evidence of a bloom is seen in the drop in nitrate levels between the March helicopter survey and the first ship-based sampling in May (Fig. 4). In contrast to SV, surface (0–50 m) nutrient inventories at RS remain relatively high during summer and usually at levels non-limiting for phytoplankton growth. These high levels are mainly the result of upwelling at the head of the Laurentian Channel and the high tidal mixing in this area, and to some degree to anthropogenic and river sources, notably from the St. Lawrence River.

This year, we include a more detailed figure showing temperature and salinity (Fig. 5) and nitrate and chlorophyll *a* (Fig. 6) conditions at RS; the high sampling frequency reveals features that are obscured during monthly averaging. The nitrate and chlorophyll figure is especially interesting: we see a pattern of low near-surface nitrate concentrations in June–July and concomitant strong pulses of chl *a* interspersed with higher nitrate/lower chl *a* values (Fig. 6). This was also seen in 2013 and 2014 but was less striking. We are investigating the possibility that this pattern has a spring–neap tidal component. We also see evidence of a small secondary

bloom in September–October 2015, but its magnitude was smaller than that of the 2014 fall bloom.

At RS, total phytoplankton and diatom abundances were near normal; flagellates and ciliates were below normal as were dinoflagellates, this latter strikingly so and for the fifth consecutive year. Consequently, the diatom/dinoflagellate ratio anomaly was strongly positive while the diatom/flagellate ratio was near normal (Fig. 7). The phytoplankton community had been regularly dominated by diatoms throughout the sampling period between 1999 and 2003, and a shift from diatoms towards flagellates and dinoflagellates was observed between 2004 and 2013 (Fig. 7). This situation changed strikingly in 2014 and 2015, with positive anomalies in the diatom/dinoflagellate ratio for the first time since 2004. Unlike 2014, where the seasonal pattern of the major phytoplankton groups was very different from the reference period (sharp increase in the relative contribution of diatoms and dinoflagellates and the near-disappearance of flagellates in fall; Devine et al. 2015), the 2015 pattern was similar to the long-term average, although the increase in the relative abundance of flagellates/decrease in that of diatoms was much more pronounced in August (Fig. 8).

The microplankton abundance anomalies at SV were all close to the long-term mean (within ~±0.5 SD). The most notable feature was the strong decline in flagellates and ciliates from 2014 to 2015 (Fig. 9). As was the case in 2014 (Devine et al. 2015), there were greater proportions of flagellates, ciliates, and dinoflagellates observed from July through December 2015 compared to the long-term mean, where diatoms had dominated the community year-round (1999–2010 reference period) (Fig. 8). Only six phytoplankton samples were analyzed at this station in 2015, so we cannot draw many generalizations from these data.

Sections and late winter helicopter survey

Late winter surface nitrate concentrations in 2015 were near normal for most regions of the GSL (Fig. 10). The highest concentrations were observed southeast of the Gaspé Peninsula and in the shallower waters south of the Laurentian Channel. This pattern is similar to that of the 2001–2015 averaged values, with concentrations gradually decreasing from west to east. No sampling was done in the SLE because of logistic constraints (lack of ice to land on), but transport of nutrient-rich water from the Estuary towards the southern GSL was evident. The winter maximum nutrient inventories in 2015 were similar to those in 2014: anomalies were mostly neutral or somewhat positive compared to the 1999–2010 average; Figs. 10, 11), thus definitively ending the period of strong negative anomalies that was evident in 2010–2011 and to a lesser extent in 2012. This is consistent with the fact that winter mixing was higher than normal in 2014 and again in 2015 (Galbraith et al. 2016).

Late spring surface nitrate inventories are always low compared to late winter inventories along the seven sections crossing the Estuary and GSL due to utilization by phytoplankton (Fig. 12). However, the magnitude of the difference between these two seasons was somewhat lower than usual in 2015. This is seen in the scorecard (Fig. 11), where anomalies in winter nitrates were mostly neutral, spring anomalies were slightly positive, and the winter–spring differences were negative. This trend is similar to the pattern observed in 2014 but somewhat attenuated. The below-average difference between the winter maximum and the late-spring minimum nitrate inventories along the sections is a trend that has been apparent since 2008 (Fig. 11). This index represents the pool of nutrients that was potentially used by phytoplankton during spring. A negative index indicates lower new phytoplankton production with potential detrimental effects on higher trophic levels. Nevertheless, spring chlorophyll anomalies in 2015—unlike 2014—were somewhat above normal for most areas (based on shipboard sampling; Fig. 11), although this is not readily apparent when examining chl *a* values averaged by section (Fig. 13).

Examination of the standardized scorecard anomalies (Fig. 11) shows a mostly coherent pattern in the seasonally adjusted (mean S+F) nitrate inventory (0–50 m), with positive or neutral anomalies everywhere except TIDM. Midwater (50–150 m) and deepwater nitrate values have shown positive anomalies since 2012, and these were even more pronounced in 2015. Spring, fall, and seasonally adjusted chlorophyll anomalies were overall above the long-term mean (except for TESL). The nitrate pattern seen for the Estuary (TESL) section (sampled twice in 2015) agrees well with that from RS (slightly above average), but not for chlorophyll *a*, which showed near-normal values at RS but negative spring and overall anomalies and slightly positive fall anomalies at TESL. RS was sampled weekly from mid-April through December (Figs. 4, 11).

Remote sensing of ocean colour

Satellite ocean colour data provide large-scale images of surface phytoplankton biomass (chl *a*) over the whole NW Atlantic. We used two-week satellite composite images of four GSL subregions to supplement our ship-based observations and provide seasonal coverage and a large-scale context over which to interpret our survey data. The ocean colour imagery provides information about the timing and spatial extent of the spring and fall blooms but does not provide information on the dynamics that take place below the top few metres of the water column. In addition, satellite ocean colour data for the St. Lawrence Estuary are largely contaminated by high concentrations of nonchlorophyllous matter originating from the continent (such as suspended particulates and coloured dissolved organic matter) that render these data too uncertain to be used. Knowledge of phytoplankton dynamics in the St. Lawrence Estuary and the subsurface information are gathered using the high-frequency sampling at Rimouski station and the broad-scale oceanographic surveys.

Satellite images in 2015 suggest that the bloom was mostly concentrated in the first part of May (Fig. 14) rather than being more spread out between mid-April and the end of May, as it was in 2014 (see Fig. 13 in Devine et al. 2015). This can be observed in the time series of the statistical subregions (Fig. 15) and is also supported by anomalies calculated for the statistical subregions, which show lower overall chlorophyll concentrations, especially in March–May, a delay in bloom initiation in the Magdalen Shallows and Cabot Strait, and generally lower-than-normal spring bloom amplitudes (all regions) and magnitudes (except NWGSL) (Fig. 16). However, notwithstanding the late start, bloom duration was higher than normal in the NEGSL while both bloom duration and magnitude were higher in the NWGSL (Fig. 16).

Satellite images from the same period as the spring mission (1–15 June 2015; Fig. 17) largely fit with the chlorophyll anomalies calculated from samples taken during the mission (30 May – 20 June 2015; Fig. 11). The composite image from early June shows a mix of negative and positive anomalies in the western area, which fits with the negative (TESL), positive (TSI), and neutral (TASO) scores, as do the neutral scores for the southern Gulf (TIDM) and Cabot Strait (TDC). However, we see no evidence in the satellite imagery for the strong positive score in the central Gulf (TCEN).

The agreement between the fall satellite image (15–31 October; Fig. 17) and anomalies calculated from the fall mission (Fig. 11) is less apparent: the anomalies are positive to varying degrees for all sections, especially TDC, whereas the satellite image shows mostly neutral or negative anomalies, except in the lower estuary and around Prince Edward Island (areas where there is no shipboard sampling). Sampling at the high-frequency monitoring site RS shows chlorophyll values close to the long-term mean and thus appears to agree more with the satellite data than with data from the fall mission. However, the scales (point samples vs. satellite images) and numbers of samples are vastly different, and thus such conclusions must be made with caution.

These apparent mismatches between satellite imagery and shipboard sampling could be due to limitations inherent in both of the methods: we have already discussed those for the imagery data, and field samples represent point values (spatially and temporally) that might not be representative of patchy events. As noted above, the satellite images record only the near-surface layer, whereas the shipboard data integrate the top 100 m of the water column, so differences may occur due to the non-uniformity of the vertical chlorophyll distribution. An additional difficulty this year is the addition of imagery data from a third source—the VIIRS satellite—which makes comparisons between imagery data (from three sources) and field measurements that much more complex.

The time series of surface chlorophyll concentrations calculated from satellite images shows that fall blooms in the GSL are generally lower in magnitude than spring blooms (Fig. 15). In 2015, the onset of the spring bloom as revealed by satellite images was delayed in the four subregions, though peak values were close to the averages. As was observed in 2014 (Devine et al. 2015), there were again fall chlorophyll peaks in the NWGSL (September) and Magdalen Shallows (October) that rivaled levels seen during the spring. Aside from the delay and the lower amplitude of the spring bloom, chlorophyll levels in the NEGSL and Cabot Strait were very near the long-term mean for the rest of the season (mid-April on; Fig. 15).

ZOOPLANKTON

High-frequency monitoring sites

The long-term patterns of zooplankton biomass at the high-frequency monitoring sites (RS: 2005–2010; SV: 1999–2010) show different seasonal patterns (Fig. 18): biomass at RS is high in April then decreases thorough the summer and increases again in late summer–fall, while that of SV increases during April–June and drops off throughout the rest of the sampling season. The zooplankton biomass at RS in 2015 was overall well below the 2005–2010 average throughout the season, which is in stark contrast to what was seen in 2014 (see Fig. 18a in Devine et al. 2015). Zooplankton biomass at SV was also generally below the average except for one very high value in late May (Fig. 18b). The sampling frequency at SV was much lower compared to RS (9 vs. 28) and so might not reveal the comprehensive pattern.

Total copepod abundance at RS in 2015 was mostly above the average throughout the sampling season (Fig. 19a). This higher-than-normal abundance of copepods corresponded to peaks in abundance of small copepod such as *Oithonia similis* in May and *Oithonia similis*, *Pseudocalanus* spp., and *Temora longicornis* in late summer; *Triconia borealis* was also more abundant than average throughout the year. In conjunction with the lower-than-normal zooplankton biomass, we noted concomitant decreases in the contributions of the large species *C. hyperboreus* and especially *C. finmarchicus* among the top 95% of identified copepod species (Fig. 19b, c). Again this year, we noted deep-dwelling species from family Aetideidae at proportions similar to those found in 2014 (Fig. 19c; see Fig. 19c in Devine et al. 2015).

At SV, the observed total copepod abundance in 2015 showed more extreme highs and lows than the average observations (Fig. 20a). The relative abundances of the dominant copepod species in 2015 showed some striking changes from the 1999–2010 average, with a peak in *Pseudocalanus* spp. in June, the first-time appearance of *Oithona atlantica* in the summer, and finally the strong and sustained presence of *Temora longicornis* starting in September (Fig. 20b). These increases in relative abundance were mirrored by the near or complete disappearance of the three *Calanus* species (*C. finmarchicus*, *C. glacialis*, *C. hyperboreus*). While *C. glacialis* and *C. hyperboreus* made considerable contributions to the copepod community in late spring over the 1999–2010 period, they were scarce in spring 2015. The most notable decrease is that of *C. finmarchicus*, which was very scarce after June (Fig. 20c).

The period of reduced abundances of *C. finmarchicus* observed at RS since 2010 continued, and the situation was even more striking in 2015: abundances were stable and well below the 2005–2010 seasonal climatology for the whole year (Fig. 21a). The peak contribution of early stages was centred in June–July, as seen in the climatology, but the proportion of early stages (CI–CIII) was much greater (Fig. 21b, c). The abundance of *C. finmarchicus* copepodite stages at SV has also been below the time-series average (1999–2010) for the past several years, and this situation appeared even more prominent in 2015 (Fig. 21d). The pattern of copepodite stages was generally similar to that observed in the long-term climatology but with a lower contribution of late development stages in the spring (Fig. 21e, f). This pattern must be interpreted with caution since there was generally only one observation per month at this station again in 2015.

The abundance of the large-bodied *C. hyperboreus* at RS in 2015 was high early in the season but roughly the same as the long-term average for the rest of the sampling period (Fig. 22a); the seasonal pattern of stage composition was also similar to the long-term average, although the appearance of the early stages seemed to be delayed by 2–3 weeks but with a normal peak abundance timing in May (Fig. 22b, c). Except for one value, abundances at SV in May and June were well below normal, whereas the species was virtually absent for the rest of the year (Fig. 22d). This absence resulted in a limited capacity to describe the seasonal pattern in stage composition at this site (Fig. 22e, f).

The abundance of *Pseudocalanus* spp. at RS was well above the time series in 2015, especially from August on (Fig. 23a). The population stage composition averaged from 2005 to 2010 showed that early stages have been observed throughout the year (potential for several generations produced by more than one species) (Fig. 23b). In 2015, copepodite CI was much more abundant in April and May than what has been observed in the 2005–2010 climatology, and the peak was shifted to earlier in the season (Fig. 23c). *Pseudocalanus* spp. abundance at SV showed high values in late May/June 2015 (markedly above the 1999–2010 average) and was both above and below average at other points in the sampling season (Fig. 23d). No stage analysis is carried out for this species at Shediac Valley.

Gulf subregions

The averaged total zooplankton biomass values during the spring and fall 2015 surveys were nearly the same and among the lowest seen over the 2000–2015 period in all three GSL subregions (Fig. 24). The same is true for the abundance of *C. finmarchicus* and *C. hyperboreus* but to a lesser degree (Fig. 25, 26). The most striking feature was the very low *C. hyperboreus* abundance in the spring in the Southern Gulf of St. Lawrence, a situation that had occurred only once over the time series (2010; Fig. 26). The 2015 abundance of *Pseudocalanus* spp. is not strikingly different from the 2000–2014 observations, which have varied widely in two (eGSL, wGSL) of the three subregions (Fig. 27). The patterns of interannual variability for these three key copepod species were similar to those observed at the high-frequency monitoring stations (c.f. RS and wGSL, SV and sGSL).

Copepod phenology

We present a detailed figure showing the seasonal cycle of the relative proportions of *C. finmarchicus* copepodite stages at Rimouski station from 1994 to 2015 in order to provide an assessment of potential changes in zooplankton phenology in the GSL (Fig. 28). The comprehensive examination of this data set revealed notable changes in the developmental timing of this key copepod species over the time series. For example, the period of maximum contribution of stages CI–III (equivalent to their abundance maximum) shifted abruptly from July (1994–2005) to June (2007–2011), with two weaker peaks of relative abundance in June and

July–August during the transition years of 2006 and 2012. The peak of these stages was seen again in late July–August for 2013–2014 before showing a protracted and earlier peak (June–mid-July) in 2015. The relative CIV abundance showed a strong peak of short duration in the 1994–2005 period that slightly lagged the CI–CIII peak, after which moderate relative abundances were seen over the season with weak peaks centred on July–August. The CV stage dominated the population from August through December throughout the time series while the CVI stage continued the long-term trend toward maximum values early in the season. Finally, the maximum relative abundance of stage CVI showed a long-term trend toward an earlier occurrence: in 2015, the period of CVI high relative abundance began in late April – early May following an apparent early development of the CV overwintering stock (Fig. 28).

Scorecards

A synthesis of standard AZMP zooplankton indices (abundances of *C. finmarchicus*, *Pseudocalanus* spp., total copepods, non-copepods) was performed using annual standardized abundance anomalies and is presented as a scorecard (Fig. 29). The reference period used to standardize annual abundances with the whole time series ranges from 1999 (2005 for RS) to 2010. In general, these annual indices were relatively coherent through the time series at RS, SV, and within the large subregions. *Calanus finmarchicus* anomalies have remained overall negative since 2009 and are even more strongly so in 2015, with the strongest negative anomaly occurring in the eGSL. The smaller *Pseudocalanus* spp. has generally shown positive abundance anomalies since 2009, with the greatest positive anomalies observed in the western regions (RS, SV, wGSL). Total copepod abundance anomalies had been negative in 2012 and 2013 but returned to normal or positive in 2015. Finally, the strong positive anomalies in non-copepod abundance that have been building in different regions since 2010 were strongly positive in all regions in 2015, especially at RS.

The annual standardized abundance anomalies for six additional zooplankton indices (*C. hyperboreous* and five zooplankton assemblages: small calanoids, large calanoids, cyclopoids, warm-water species, and cold/arctic species) are presented in Figure 30. Again, these annual indices were relatively coherent among the high-frequency sampling sites (RS, SV) and GSL subregions over the time series. The abundances of small calanoids and especially warm-water copepods all showed positive anomalies, while abundance anomalies for large calanoids and cold-water copepods tended toward more negative values. *Calanus hyperboreous* anomalies in all areas switched from positive to neutral or negative in 2015, and cyclopoid anomalies were about the same as in 2014. Lower-than-normal abundances of large calanoids have been the norm in the GSL since 2009 (except for 2012), and this trend intensified over all regions in 2015. Small calanoid abundances were above normal in 2015 (Fig. 30), likely because of the high abundances of *Pseudocalanus* spp. (positive anomalies characterized the whole GSL; Fig. 29); we also saw a large increase in *Temora longicornis* at SV (Fig. 20). There were two striking results revealed by the 2015 scorecard. One was the strong positive anomalies for warm-water species and small calanoids in all regions (Fig. 30). The other was the abundances of large calanoids, *C. hyperboreous*, and cold/arctic copepod species (*C. glacialis*, *M. longa*): all of these moved toward negative and often strongly negative anomies compared to the last few years (except cold-water copepods in RS and eGSL; Fig. 30). Note that indices of warm-water and cold/arctic species are based on generally rare taxa, implying that relatively minor changes in abundance could result in large variations in their anomalies.

DISCUSSION

Galbraith et al. (2016) published a report on the physical conditions in the GSL in 2015. Among the key findings of that report, we note that freshwater runoff in the St. Lawrence River

(measured at Québec City) was below normal, that the sea-ice concentration was above normal, and that the sea-surface temperatures were generally below normal until July and above normal from August to September, leading to near-normal May–November conditions. This represents a warming in the first part of the year compared to overall colder conditions that had been reported in 2014 (Galbraith et al. 2015). Deepwater temperatures for 2014 were high, and the increasing trend continued (to record highs) in 2015. The report of Galbraith et al. (2016) includes a figure that provides an integrated summary of many of these physical variables; we reproduce it here for convenience (Fig. 31) .This document reports on the chemical and biological conditions in the GSL in the context of these conditions.

Winter maximum surface nutrient inventories in 2015 were close to the 2001–2010 average throughout the GSL after a period of strong negative anomalies that was evident in 2010–2011. Spring and fall nutrient inventories were somewhat above normal in most regions, while seasonal averages were above normal, especially so in the deeper waters (50–150 m, 300 m). Winter mixing is a critical process for bringing nutrient-rich deep water to the surface. In the GSL, this winter convection is in part caused by buoyancy loss (cooling and reduced runoff), brine rejection associated with sea-ice formation, and wind-driven mixing prior to ice formation (Galbraith 2006). Thus, physical conditions in the Gulf led to a higher initial supply of nutrients for primary producers in 2015 compared to the 2010–2011 period. In addition to vertical mixing, upwelling at the head of the Laurentian Channel and the transport of nutrients via the Gaspé Current may also have contributed to enhancing winter nutrient inventories for the estuarine portion and freshwater-influenced subregions of the GSL.

Water intrusions into Cabot Strait from south of Newfoundland were near normal in 2015 (Galbraith et al. 2016). Typically, these waters—which enter the Gulf via Cabot Strait during winter and flow in part northward along the west coast of Newfoundland—are relatively poor in nutrients compared to those that originate in the Estuary or are mixed from deeper waters within the Gulf. As mentioned above, increasingly high positive nutrient anomalies in the intermediate (50–150) and deep (300 m) waters have been observed since 2012 in all areas. These higher-than-average deeper inventories are probably associated with a combination of the above-normal winter mixed-layer depth, the thermocline that is higher in the water column, and the water mass composition that has a greater contribution of Gulf Stream water than Labrador Shelf water (Galbraith et al. 2016).

In contrast to expectations based on winter nutrient inventories, ocean colour data as well as the spring nitrate inventories revealed that the magnitude of the spring phytoplankton bloom in 2015 was below normal and of shorter duration across the region. In addition, phytoplankton growth in the southern part of the Gulf was initiated later than in recent years. The below-normal spring freshet combined with the delayed warming of surface waters and delayed intrusion of water from the Labrador Shelf (Galbraith et al. 2016) could be related to changes in bloom dynamics. In addition, ice conditions were above normal: changes in ice cover can influence primary production by its effect on the light conditions in the water column (Le Fouest et al. 2005), and changes in stratification can also have either positive or negative effects on primary production depending on water column conditions (Ferland et al. 2011). Thus, the later-than-normal ice retreat and later warming/stratification (Galbraith et al. 2016) contributed to the delayed spring bloom in 2015 compared to recent years. The fact that utilization of nutrients during the spring was overall below normal in 2015 is consistent with this interpretation. Late summer and fall chlorophyll *a* levels were near normal in most regions of the GSL, coinciding with the warming of surface waters (Galbraith et al. 2016).

The timing of the spring bloom in the St. Lawrence Estuary is known to be largely influenced by both runoff intensity and freshwater-associated turbidity (Levasseur et al. 1984, Therriault and Levasseur 1985; Zakardjian et al. 2000, Le Fouest et al. 2010, Mei et al. 2010). The spring

bloom typically starts just after the spring–summer runoff peak, and this was the case in 2015. The smaller-than-normal and somewhat delayed peak runoff value (Galbraith et al. 2016) is likely responsible for the delayed and protracted peak of chl *a* in the NWGSL. In this context, the unexpected above-normal phytoplankton biomass from May onward suggests that the phytoplankton growth rate largely compensated for losses due to physical transport (advection) and biological factors such as grazing by zooplankton, which could have been lower than usual in 2015 (see below).

The shift to a smaller-sized phytoplankton community observed in recent years at Rimouski station reversed in 2014 and 2015, with strongly positive anomalies in the diatom/flagellate ratio for the first time since 2004. This likely resulted from decreased abundances in flagellates, ciliates, and especially dinoflagellates compared to near-normal abundances of diatoms, since the overall phytoplankton anomaly was slightly negative. This shift is consistent with the slightly above-normal phytoplankton biomass and nutrient inventory in the region during fall. Diatoms are usually largely responsible for major changes in chlorophyll biomass and are associated with a nutrient-rich, well-mixed environment. In contrast, flagellates and dinoflagellates are associated with a nutrient-poor, stratified environment. In this context, it is interesting to note that the situation at SV in 2015 was very different from that at RS: diatom and flagellate abundances were lower compared to the long-term average while dinoflagellates and ciliates showed weak positive anomalies. Warmer temperatures and stronger stratification, as observed in summer 2014 in the GSL but less so in the SLE (RS) (Galbraith et al. 2015), are associated with a shift toward greater flagellate and dinoflagellate predominance (Levasseur et al. 1984, Li and Harrison 2008), with potential consequences on copepod recruitment and zooplankton composition as well as on the flow of energy in marine food webs. However, while temperatures were above normal in 2015 at both SV and RS, stratification was weak (Galbraith et al. 2016), which could help explain the shift back toward relatively greater diatom abundances.

In 2015, deepwater temperatures and salinities were reported to be overall well above normal in the Gulf because of inward advection from Cabot Strait, where temperature and salinity had reached record highs in 2012 at 200 and 300 m (Galbraith et al. 2016). The above-normal deep (300 m) nutrient levels that we observed are associated with this water mass. These elevated values of temperature, salinity, and nutrients indicate that a higher proportion of slope water compared to Labrador Shelf water was entering the GSL. Since this appears to be a recurrent event over the last few years (Galbraith et al. 2016), further investigation is clearly needed on this phenomenon. The warming of bottom waters and their above-normal nutrient levels (which will eventually be upwelled at the head of the Laurentian Channel) may have impacts on acidification previously reported in the region (Mucci et al. 2011), with potential negative consequences on fisheries and aquaculture activities as well as on overall productivity and biodiversity in the GSL.

The zooplankton community and key species dynamics in the region reflected both the tendency observed during the previous years and the environmental conditions observed in 2015. The most striking feature in 2015 was the strong negative anomaly in *C. finmarchicus* and the highly positive anomaly in *Pseudocalanus* spp. across the region, confirming the trend observed during previous years and the prevalence of below- and above-normal abundances of large and small calanoids, respectively. In deeper regions of the wGSL and eGSL (including RS), the sustained below-normal abundance of both *C. finmarchicus* (since 2009) and of the cold-water *C. glacialis* might have favoured the recruitment of *Pseudocalanus* spp. in spring and early summer by diminishing competition for adequate food. The same applies to SV and eGSL, where the greater-than-normal contributions of *Pseudocalanus* and *Temora longicornis* were concomitant to very low abundances of *C. finmarchicus* and *C. hyperboreus*. Lower-than-normal phytoplankton biomass in spring and summer–fall might have also limited the productivity of

large-bodied *Calanus* spp., which have life-cycle strategies that are more associated with the offshore spring phytoplankton bloom than is the case for their small-bodied neritic and opportunistic counterparts. Finally, local environmental conditions (lower-than-normal freshet, earlier timing of spring bloom in wGSL, above-normal deepwater temperature; Galbraith et al. 2016) likely conditioned a much earlier timing of *C. finmarchicus* development at RS compared to previous years, with potential consequences on upper trophic levels.

In 2013, deepwater temperatures and salinity averaged over the Gulf increased slightly to reach the highest values since 1980 (Galbraith et al. 2014). This warm anomaly was first observed in Cabot Strait and has propagated northwestward into the Gulf; it was observed at RS in 2015 for the second consecutive year (Galbraith et al. 2016). Combined with surface water temperatures that were again well above normal in the eGSL and wGSL in summer, these conditions likely resulted in the well-above-normal (RS, wGSL, eGSL) abundances of warm-water copepod species in 2015. These high positive anomalies in deeper regions of the wGSL and eGSL and at RS were mostly caused by the high abundance of *M. lucens*, an oceanic species that performs strong diel vertical migrations and is mostly restricted to deep regions. This species is mostly associated with temperate conditions and thus might have benefited from a warmer and saltier deep layer as well as from warmer conditions at the surface typical of recent years in the Gulf. These high positive anomalies of warm-water copepod species were due to higher abundances of surface-dwelling and neritic *Paracalanus* spp. and *Centropages* spp. in the eGSL and sGSL, respectively. These two taxa showed strong interannual variabilities that are likely related to high-frequency variations in upper-ocean environmental conditions, whereas the deepwater *M. lucens* exhibited high anomalies over the last four to five years, likely associated with lower-frequency variations of the more stable deepwater characteristics (Galbraith et al. 2016). The warmer-than-normal deep waters at RS in 2015 might also explain the above-normal abundance of Aetideidae, a family composed of various deep-dwelling copepod species generally associated with deep oceanic regions.

Contrary to 2014, when cold-water copepod species (*C. glacialis*, *M. longa*) showed near-normal abundances across the region, 2015 showed a less consistent signal, with below-normal abundances in the wGSL and sGSL (including SV) and positive anomalies at RS and in the eGSL. Environmental conditions that might favour the reproduction and recruitment of cold-water zooplankton species such *C. glacialis* and *M. longa* were either near normal (seasonal ice cover) or below normal (warmer and thinner CIL, lower phytoplankton biomass in spring), whereas temperatures well above normal were the norm in deep waters and in the surface layer in summer and fall 2015 (see Fig. 16 in Galbraith et al. 2016). Moreover, lower-than-normal phytoplankton biomass in summer and fall might be detrimental to *M. longa* recruitment because their mesopelagic early copepodite stages probably exploit sinking phytoplankton aggregates and associated microfauna during their development (Grønvik and Hopkins 1984, Plourde et al. 2002).

In 2015, all *C. finmarchicus* abundance indices showed strong negative anomalies for the seventh consecutive year, with abundance being particularly low in the eGSL. These strong negative anomalies in the Gulf and in the eGSL in particular could have resulted from a suite of environmental conditions that were detrimental to the *C. finmarchicus* population. First, the abundance of *C. finmarchicus* was predominantly well below its long-term average in 2015 on the Newfoundland Shelf, an area upstream of Cabot Strait and representing the proximate source for the Gulf population (Maps et al. 2011, DFO 2016). Second, surface phytoplankton biomass during the spring bloom was well below normal across the Gulf, with potentially negative consequences on the production of the new generation that would not have been compensated later in the season due to the near-normal post-bloom phytoplankton biomass and warm conditions that prevailed in the region in summer and fall 2015 (Galbraith et al. 2016).

Finally, a massive cohort of the local redfish stock (*Sebastes mentella*) first detected in 2013 was observed again in 2015, with the occurrence of 15–20 cm individuals (three or four years old) mainly located in the deep channels between 150 and 200 m of depth (Bourdages et al. 2015; I. McQuinn, DFO, Mont-Joli, Qc, unpublished data). Given that small redfish (< 25 cm) feed predominantly on large calanoids and other small crustaceans (Gonzalez et al. 2000), it is possible that this redfish cohort represents a predatory threat that could exert a significant top-down pressure on the GSL *C. finmarchicus* overwintering population not observed since the early 1980s in the region.

SUMMARY

This document reports on the chemical and biological (plankton) conditions in the GSL in 2015 in the context of a strong warming event initiated in 2010 but with delayed warming and freshwater runoff in 2015. Data from 2015 are compared to time-series observations.

- Nutrient inventories averaged over sampling sections in 2015 were near or slightly above normal in the 0–50 m layer and strongly above normal in the deeper layers. For a fourth consecutive year, highly positive deepwater (> 200 m) nitrate concentrations were associated with high temperature and salinity.
- Compared to the 1999–2010 time series, the spring bloom began earlier, lasted longer, and had a greater magnitude in the NWGSL and NEGSL while the reverse was observed for the Magdalen Shallows and Cabot Strait, consistent with the late retreat of sea-ice in those regions.
- The difference between winter (maximum) and late spring (minimum) nitrate inventories was below normal in many regions of the GSL, which is inconsistent with higher-than-normal primary production (as estimated by chlorophyll a biomass) measured during the June survey in 2015. Nevertheless, satellite ocean colour data indicate that productivity was lower in the four Gulf subregions, while chlorophyll biomass at the two high-frequency monitoring sites was near normal throughout the year.
- The shift to a smaller-sized phytoplankton community that had been observed from 2004 to 2013 at Rimouski station continued the reversal first observed 2014, with a second year of positive anomalies in the diatom/flagellate ratios in 2015. This was largely due to the protracted high relative contribution of diatoms in fall and a scarcity of dinoflagellates throughout the season. Conversely, the smaller-sized phytoplankton community was evident at Shediac Valley, with increased relative abundances of dinoflagellates and ciliates in 2015.
- Zooplankton biomass was below normal at the two long-term monitoring sites as well as in the three Gulf regions sampled during the spring and fall missions. Specifically, there were strong declines in the indices for *C. finmarchicus*, large calanoids, and cold-water copepods and strong increases in *Pseudocalanus* spp., small calanoids, warm-water copepods, and non-copepods.
- The abundance of *C. finmarchicus* was below normal for the seventh consecutive year (since 2009), whereas the small calanoids copepod *Pseudocalanus* spp. has shown abundances predominantly above normal since 2010.
- The overall high Gulf-wide temperatures (surface and deep layers) and salinities observed in 2015 likely led to the well-above-normal abundances of warm-water copepod species (*M. lucens*, *Paracalanus* spp., and *Centropages* spp.) as well as the presence of specimens from the family Aetideidae, which appeared in the top 95% most abundant copepod taxa for the first time in 2014.

ACKNOWLEDGEMENTS

We thank Jean-Yves Couture and Sylvie Lessard as well as Isabelle St-Pierre and Caroline Lafleur for preparation and standardization of the phytoplankton and zooplankton data, respectively. The data used in this report would not be available without the work of François Villeneuve and his team (Sylvain Chartrand, Rémi Desmarais, Marie-Lyne Dubé, Yves Gagnon, Line McLaughlin, Roger Pigeon, Michel Rousseau, Félix St-Pierre, Daniel Thibault, and the late Sylvain Cantin) in organizing and carrying out AZMP cruises and analyzing samples. Marie-France Beaulieu performed all zooplankton sample analyses. We thank Jeff Spry for providing data from the Shediac Valley station and BIO's remote sensing unit for the composite satellite images. We are grateful to Catherine Johnson and Pierre Pepin for their critical reviews.

REFERENCES

Arun Kumar, S.V.V., Babu, K.N., and Shukla, A.K. 2015. Comparative analysis of chlorophyll-a distribution from SeaWiFS, MODIS-Aqua, MODIS-Terra and MERIS in the Arabian Sea. Mar. Geod. 38: 40–57.

AZMP. 2006. Physical and biological status of the environment. AZMP Bulletin PMZA 5: 3–8.

Barnes, B., and Hu, C. 2016. Dependence of satellite ocean color data products on viewing angles: A comparison between SeaWiFS, MODIS, and VIIRS. Remote Sens. Environ. 175:120–129.

Bourdages, H., Brassard, C., Desgagnés, M., Galbraith, P., Gauthier, J., Lambert, J., Légaré, B., Parent, E., and Schwab, P. 2015. Preliminary results from the groundfish and shrimp multidisciplinary survey in August 2014 in the Estuary and northern Gulf of St. Lawrence. DFO Can. Sci. Advis. Sec. Res. Doc. 2014/115. v + 96 p.

Brickman, D., and Petrie, B. 2003. Nitrate, silicate and phosphate atlas for the Gulf of St. Lawrence. Can. Tech. Rep. Hydrogr. Ocean Sci. 231: xi + 152 pp.

Devine, L., Plourde, S., Starr, M., St-Pierre, J.-F., St-Amand, L., Joly, P., and Galbraith, P.S. 2015. Chemical and biological oceanographic conditions in the Estuary and Gulf of St. Lawrence during 2014. DFO Can. Sci. Advis. Sec. Res. Doc. 2015/071. v + 46 pp.

DFO. 2016. Oceanographic conditions in the Atlantic zone in 2015. DFO Can. Sci. Advis. Sec. Sci. Advis. Rep. 2016/041.

Ferland, J., Gosselin, M., and Starr, M. 2011. Environmental control of summer primary production in the Hudson Bay system: The role of stratification. J. Mar. Syst. 88(3): 385–400.

Galbraith, P. S. 2006. Winter water masses in the Gulf of St. Lawrence. J. Geophys. Res. 111, C06022, doi:10.1029/2005JC003159.

Galbraith, P. S., Desmarais, R., Pigeon, R., and Cantin, S. 2006. Ten years of monitoring winter water masses in the Gulf of St. Lawrence by helicopter. AZMP Bulletin PMZA 5: 32–35.

Galbraith, P. S., Chassé, J., Gilbert, D., Larouche, P., Caverhill, C., Lefaivre, D., Brickman, D., Pettigrew, B., Devine, L., and Lafleur, C. 2014. Physical oceanographic conditions in the Gulf of St. Lawrence in 2013. DFO Can. Sci. Advis. Sec. Res. Doc. 2014/062. vi + 84 p.

Galbraith, P. S., Chassé, J., Nicot, P., Caverhill, C., Gilbert, D., Pettigrew, B., Lefaivre, D., Brickman, D., Devine, L., and Lafleur, C. 2015. Physical oceanographic conditions in the Gulf of St. Lawrence in 2014. DFO Can. Sci. Advis. Sec. Res. Doc. 2015/032. v + 82 p.

Galbraith, P.S., Chassé, J., Caverhill, C., Nicot, P., Gilbert, D., Pettigrew, B., Lefaivre, D., Brickman, D., Devine, L., and Lafleur, C. 2016. Physical Oceanographic Conditions in the Gulf of St. Lawrence in 2015. DFO Can. Sci. Advis. Sec. Res. Doc. 2016/056. v + 90 p.

Gonzalez, C., Bruno, I., and Paz, X. 2000. Food and feeding of deep-sea redfish (*Sebastes mentella* Travin) in the North Atlantic. NAFO Sci. Coun. Studies 33: 89–101.

Gregg, W. W., and Rousseaux, C. S. 2014. Decadal trends in global pelagic ocean chlorophyll: A new assessment integrating multiple satellites, in situ data, and models. J. Geophys. Res. Oceans, 119: 5921–5933, doi 10.1002/2014JC010158.

Grønvik, S., and Hopkins, C. C. E. 1984. Ecological investigations of the zooplankton community of Balsfjorden, northern Norway: Generation cycle, seasonal vertical distribution, and seasonal variations in body weight and carbon and nitrogen content of the copepod *Metridia longa* (Lubbock). J. Exp. Mar. Biol. Ecol. 80: 93–107.

Le Fouest, V., Zakardjian, B., Saucier, F., and Starr, M. 2005. Seasonal versus synoptic variability in planktonic production in a high-latitude marginal sea: the Gulf of St. Lawrence (Canada). J. Geophys. Res. 110, C09012, doi 10.1029/2004JC002423.

Le Fouest, V., Zakardjian, B., and Saucier, F. J. 2010. Plankton ecosystem response to freshwater-associated bulk turbidity in the subarctic Gulf of St. Lawrence (Canada): A modelling study. J. Mar. Syst. 81(1-2): 75–85.

Levasseur, M., Therriault, J.-C., and Legendre, L. 1984. Hierarchical control of phytoplankton succession by physical factors. Mar. Ecol. Prog. Ser. 19: 211–222.

Li, W. K. W., and Harrison, W. G. 2008. Propagation of an atmospheric climate signal to phytoplankton in a small marine basin. Limnol. Oceanogr. 53(5): 1734–1745.

Maps, F., Zakardjian, B., Plourde, S., and Saucier, F. J. 2011. Modeling the interactions between the seasonal and diel migration behaviors of *Calanus finmarchicus* and the circulation in the Gulf of St. Lawrence (Canada). J. Mar. Syst. 88: 183–202.

Mei, Z.-P., Saucier, F., Le Fouest, V., Zakardjian, B., Sennville, S., Xie, H., and Starr, M. 2010. Modeling the timing of spring phytoplankton bloom and biological production of the Gulf of St. Lawrence (Canada): Effects of colored dissolved organic matter and temperature. Cont. Shelf Res. 30: 2027–2042.

Mitchell, M. R., Harrison, G., Pauley, K., Gagné, A., Maillet, G., and Strain, P. 2002. Atlantic Zonal Monitoring Program sampling protocol. Can. Tech. Rep. Hydrogr. Ocean Sci. 223: iv + 23 pp.

Mucci, A., Starr, M., Gilbert, D., and Sundby, B. 2011. Acidification of lower St. Lawrence Estuary bottom waters. Atmos.-Ocean 49(3): 206–218.

Plourde, S., Dodson, J. J., Runge, J. A., and Therriault, J.-C. 2002. Spatial and temporal variations in copepod community structure in the lower St. Lawrence Estuary, Canada. Mar. Ecol. Prog. Ser. 230: 221–224.

Plourde, S., Maps, F., and Joly, P. 2009. Mortality and survival in early stages control recruitment in *Calanus finmarchicus*. J. Plankton Res. 31(4): 371–388.

Therriault, J.-C., and Levasseur, M. 1985. Control of phytoplankton production in the Lower St. Lawrence Estuary: light and freshwater runoff. Nat. Can. 112: 77–96.

Therriault, J.-C., Petrie, B., Pépin, P., Gagnon, J., Gregory, D., Helbig, J., Herman, A., Lefaivre, D., Mitchell, M., Pelchat, B., Runge, J., and Sameoto, D. 1998. Proposal for a Northwest Atlantic zonal monitoring program. Can. Tech. Rep. Hydrogr. Ocean Sci. 194: vii + 57 pp.

Wang, M., Liu, X., Tan, L., Jiang, L., Son, S. H., Shi, W., Rausch, K., and Voss, K. 2013. Impacts of VIIRS SDR performance on ocean color products. J. Geophys. Res. Atmos. 118: 10,347–10,360, doi:10.1002/jgrd.50793.

Welschmeyer, N. A. 1994. Fluorometric analysis of chlorophyll *a* in the presence of chlorophyll *b* and pheopigments. Limnol. Oceanogr. 39(8): 1985-1992.

Zakardjian, B. A., Gratton, Y., and Vézina, A. F. 2000. Late spring phytoplankton bloom in the Lower St. Lawrence Estuary: the flushing hypothesis revisited. Mar. Ecol. Prog. Ser. 192: 31–48.

Zhai, L., Platt, T., Tang, C., Sathyendranath, S., and Hernández Walls, R. 2011. Phytoplankton phenology on the Scotian Shelf. ICES J. Mar. Sci. 68: 781–791 (doi:10.1093/icesjms/fsq175).

Zibordi, G., Mélin, F., and Berthon, J.-F. 2006. Comparison of SeaWiFS, MODIS and MERIS radiometric products at a coastal site. Geophys. Res. Letters 33: L06617, doi:10.1029/2006GL025778.

TABLES

Table 1. List of AZMP missions with locations, dates, and sampling activities for 2015. wGSL, eGSL, and sGSL denote the western, eastern, and southern subregions of the Gulf of St. Lawrence. See Figure 1 for station locations.

Sampling group	Name	Location	Dates (2015)	Vessel	CTD/bottle	Net
Fixed	Rimouski	48°40.0'N 068°35.0'W	22 Apr–16 Dec	Beluga II	30	28
	Shediac Valley	47°46.8'N 064°01.8'W	09 Mar–09 Dec	Multiple	10	9
Spring Sections	TESL	wGSL	30 May–20 Jun	Teleost	7	7
	TSI	wGSL	30 May–20 Jun	Teleost	6	5
	TASO	wGSL	30 May–20 Jun	Teleost	5	5
	TIDM	sGSL	30 May–20 Jun	Teleost	10	10
	TDC	eGSL	30 May–20 Jun	Teleost	5	5
	TCEN	eGSL	30 May–20 Jun	Teleost	3	3
	TBB	eGSL	30 May–20 Jun	Teleost	7	7
Total					43	42
Fall Sections	TESL	wGSL	19 Oct–06 Nov	Hudson	7	7
	TSI	wGSL	19 Oct–06 Nov	Hudson	6	6
	TASO	wGSL	19 Oct–06 Nov	Hudson	5	5
	TIDM	sGSL	19 Oct–06 Nov	Hudson	10	10
	TDC	eGSL	19 Oct–06 Nov	Hudson	6	6
	TCEN	eGSL	19 Oct–06 Nov	Hudson	5	5
	TBB	eGSL	19 Oct–06 Nov	Hudson	7	7
Total					46	46

FIGURES

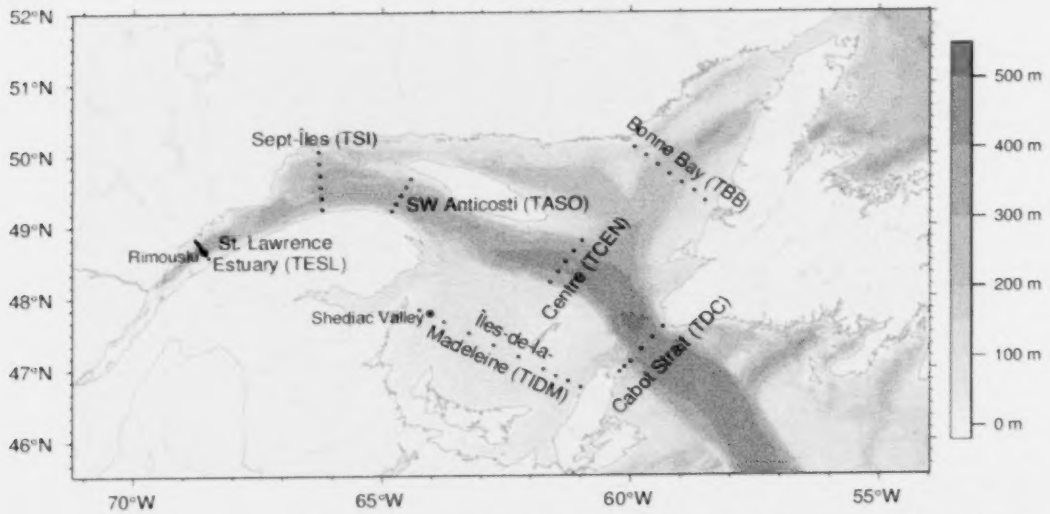

Figure 1. Bathymetric map of the Estuary and Gulf of St. Lawrence showing sampling stations on the different sections (dots) and at Rimouski and Shediac Valley stations (circles). Sections were grouped to form subregions: TESL, TSI, TASO: western GSL; TIDM: southern GSL; TBB, TCEN, TDC: eastern GSL.

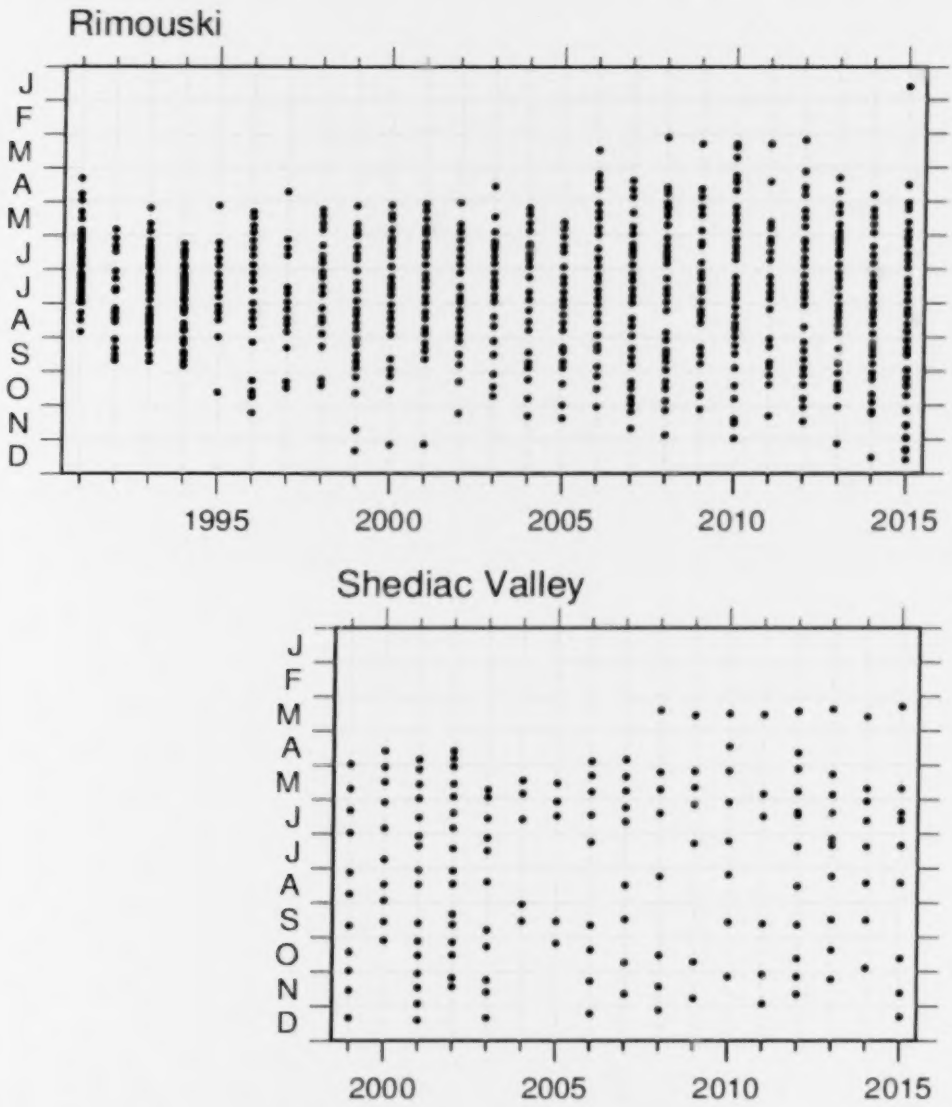

Figure 2. Sampling frequencies at Rimouski and Shediac Valley stations showing bottle and net sampling effort through 2015.

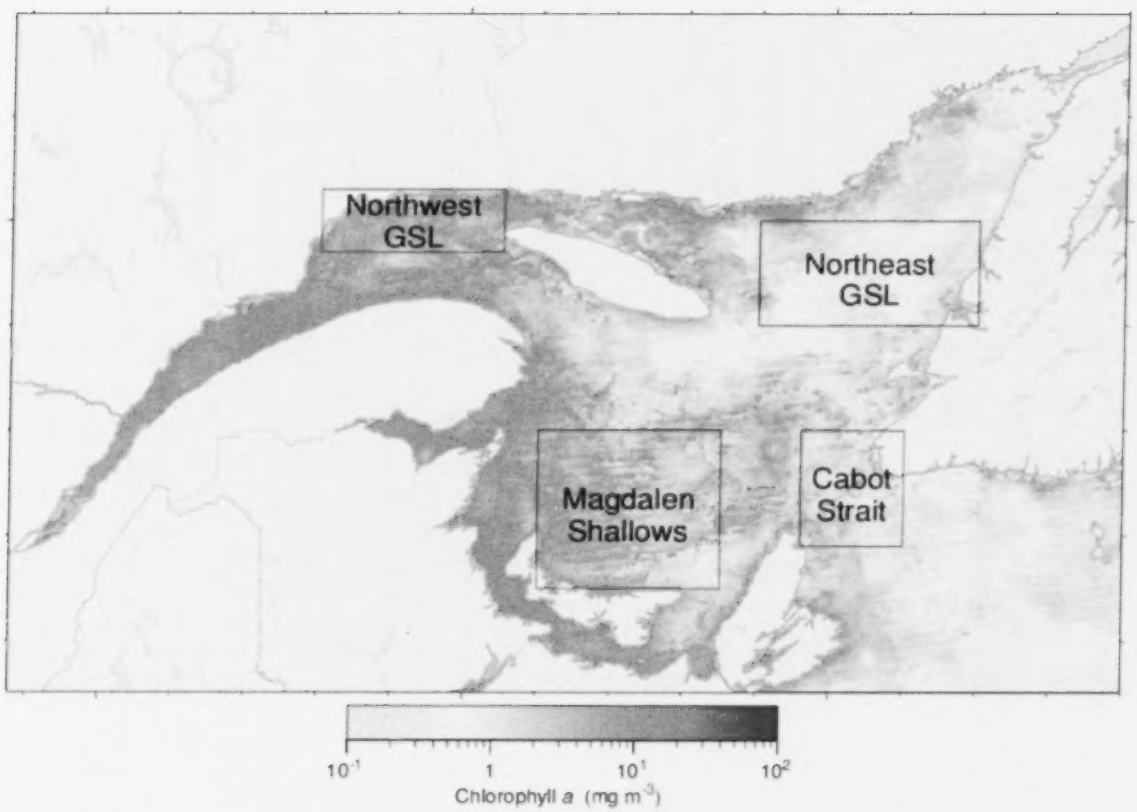

Figure 3. Statistical subregions in the Gulf of St. Lawrence (GSL) identified for the spatial/temporal analysis of satellite ocean colour data. The figure is a MODIS composite image showing chlorophyll a from 1–15 May 2015. Gray areas indicate no data (in this case because of ice; near-shore regions are also excluded).

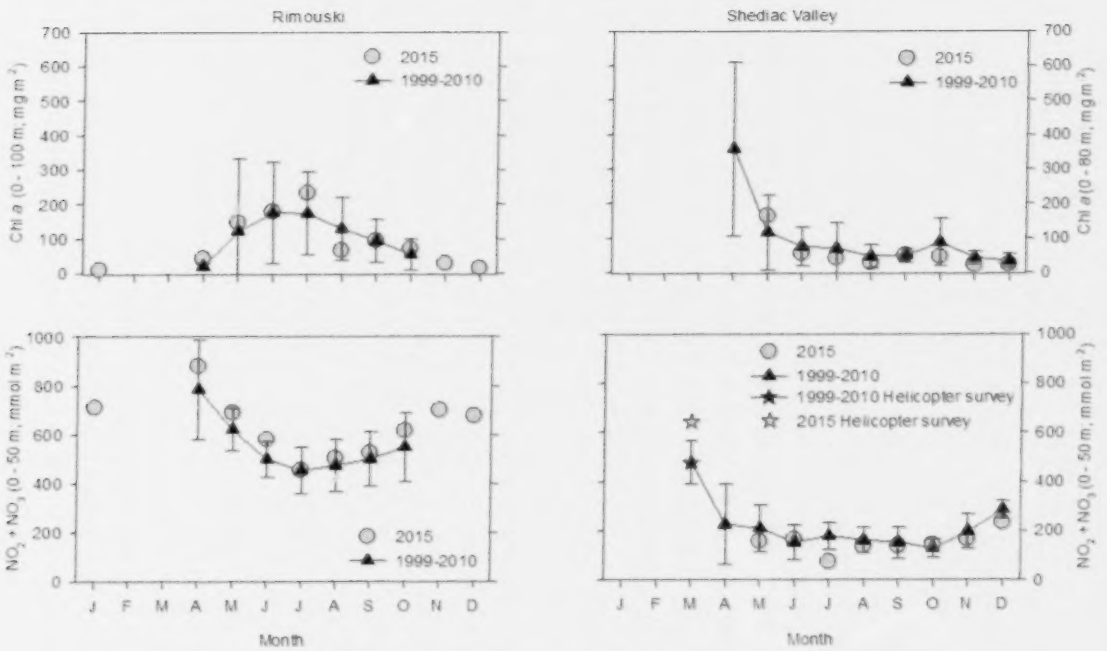
Rimouski
Shediac Valley
2015
1999-2010
1999-2010 Helicopter survey
2015 Helicopter survey
Chl a (0 - 100 m, mg m-2)
Chl a (0 - 80 m, mg m-2)
NO2 + NO3 (0 - 50 m, mmol m-2)
J F M A M J J A S O N D
Month

Index	Units	Depth (m)	Station	1999	2000	2001	2002	2003	2004	2005	2006	2007	2008	2009	2010	2011	2012	2013	2014	2015	Mean	SD
Chl a	mg m^{-2}	0–100	Rimouski	NA	-0.23	0.04	-0.28	0.48	-0.76	-0.41	-0.47	0.50	-0.89	0.24	0.02	-0.28	0.55	0.13	1.39	0.36	109	58
		0–80	Shediac Valley	-0.44	-0.70	-0.25	1.13	0.23	-0.46	-0.56	-0.13	0.46	0.60	0.14	-0.25	-0.65	-0.09	0.73	-0.19	-0.47	97	73
$NO_3 + NO_2$	mmol m^{-2}	0–50	Rimouski	-0.35	0.61	0.07	1.13	-0.30	0.85	-0.29	0.00	-0.07	0.43	-0.44	-1.32	-0.62	-0.28	0.08	0.28	0.47	554	115
			Shediac Valley	0.23	0.66	-0.32	0.16	0.16	0.55	-0.23	0.66	-1.15	-0.09	0.66	-1.18	-0.85	0.18	-0.40	0.12	-0.60	188	71
		50–150	Rimouski	NA	-0.27	0.54	0.95	-0.68	-0.12	-0.26	0.61	0.67	-0.39	0.18	-1.18	-1.06	0.14	-0.73	0.96	0.62	1471	45
		50–80	Shediac Valley	-0.15	1.01	0.17	0.67	-0.06	0.53	-0.17	0.61	-1.17	0.12	-0.09	-1.39	-1.50	-0.43	-0.96	-0.44	-0.18	275	65

Figure 4. Chlorophyll a levels (0–100 m Rimouski and 0–80 m Shediac Valley; top panels) and nitrate inventories (0–50 m; bottom panels) in 2015 (circles) with mean conditions from 1999–2010 (triangles) at Rimouski and Shediac Valley stations. Vertical lines are the 95% confidence intervals of the monthly mean. The March nitrate values at Shediac Valley are from the helicopter survey (samples from 2 m). Normalized annual anomalies (scorecard) for chlorophyll a levels (mg m^{-2}) and nutrient inventories (mmol m^{-2}) are also presented with the variables' means and standard deviations. Blue colours indicate anomalies below the mean and reds are anomalies above the mean.

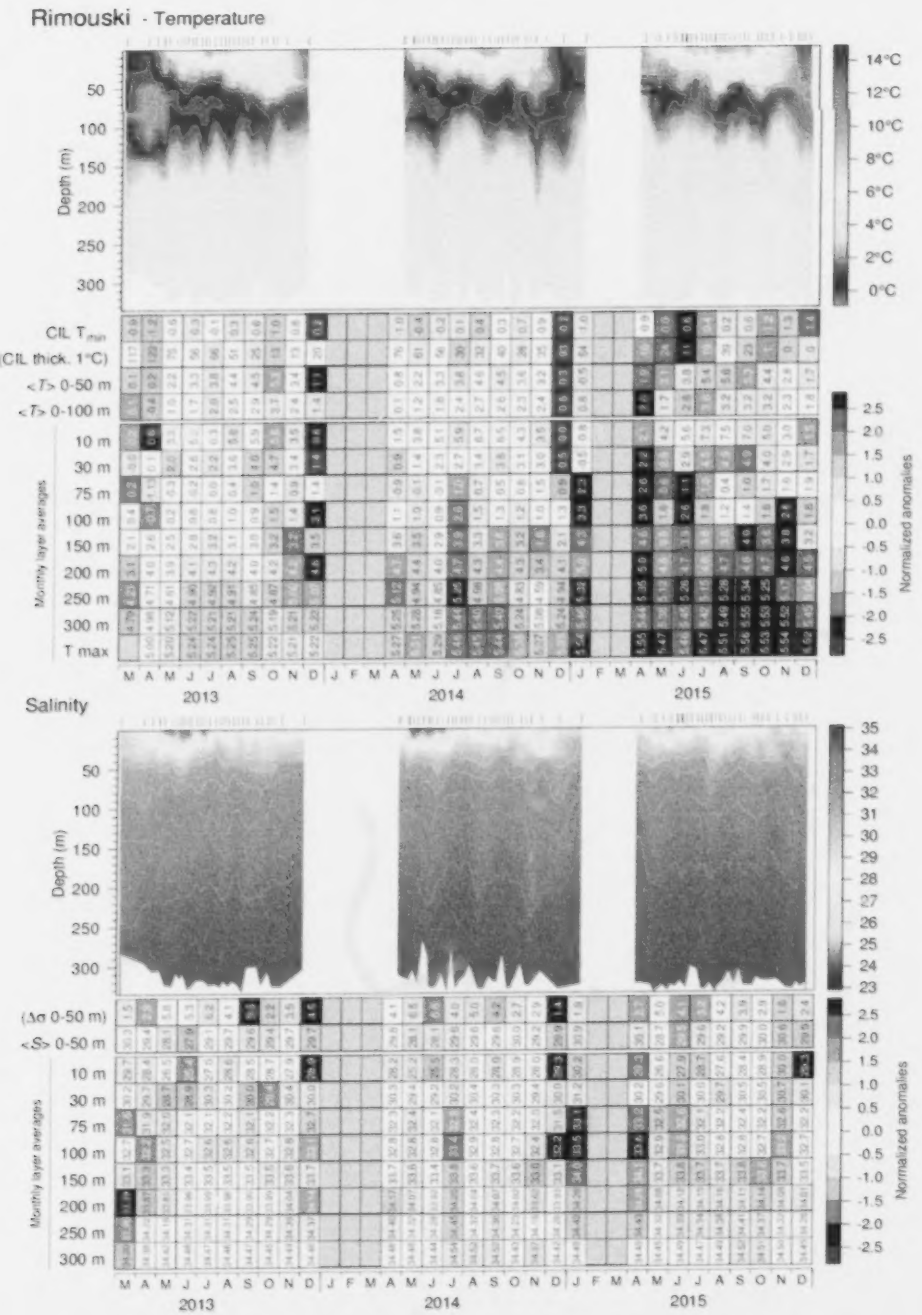

Figure 5. Temperature (top) and salinity (bottom) concentrations at Rimouski station during the 2013 to 2015 sampling seasons. Contour plots are made with data from individual sorties while monthly means are shown in the tables below the graphics. Cell colours indicate normalized anomalies based on the 1991–2010 climatology: blue colours indicate anomalies below the mean and reds are anomalies above the mean.

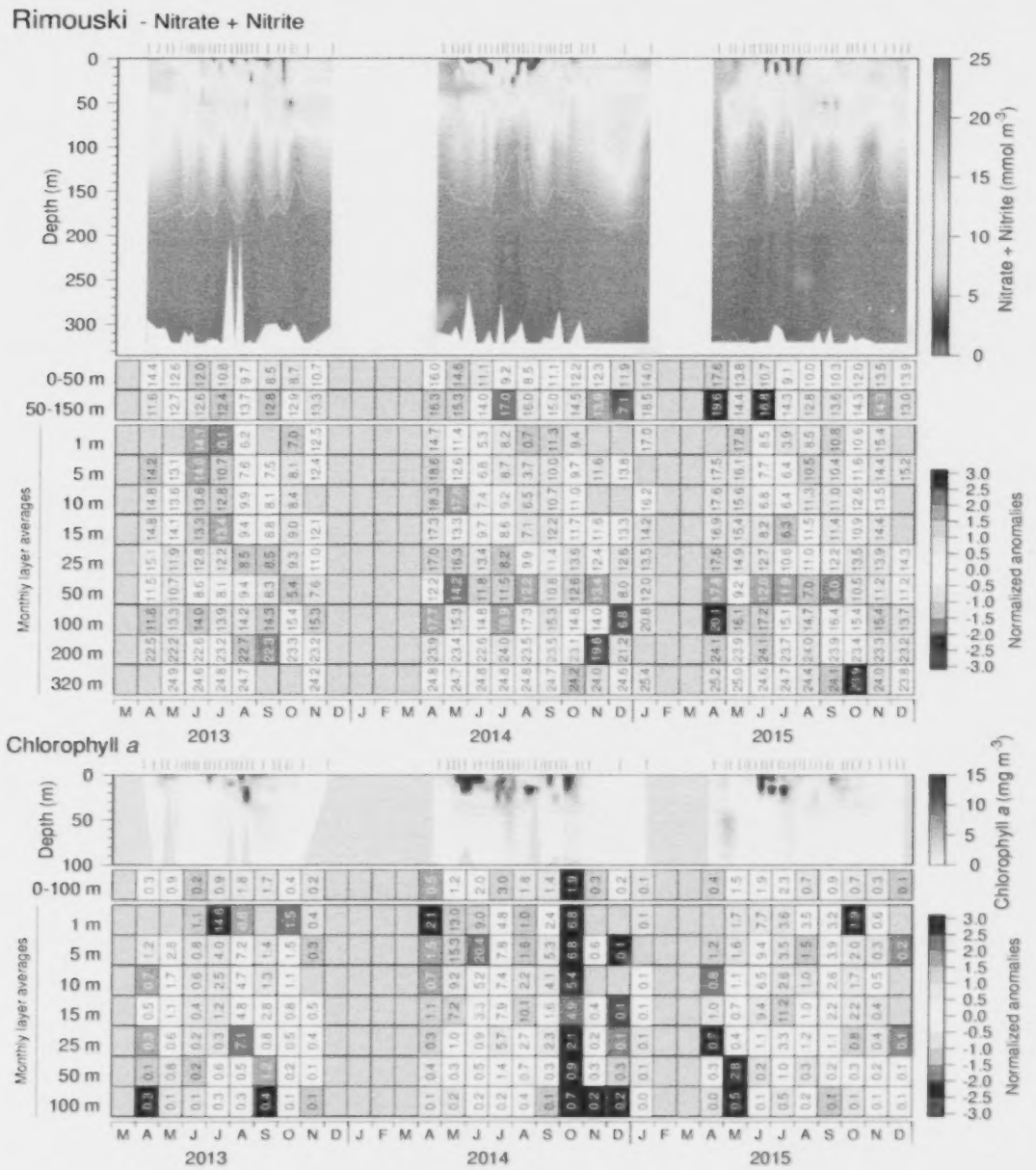

Figure 6. Nitrate (top) and chlorophyll a (bottom) concentrations at Rimouski station during the 2013 to 2015 sampling seasons. Contour plots are made with data from individual sorties while monthly means are shown in the tables below the graphics (nitrates: mmol m^{-3}; chl a: mg m^{-3}). Cell colours indicate normalized anomalies based on the 1991–2010 climatology: blue colours indicate anomalies below the mean and reds are anomalies above the mean.

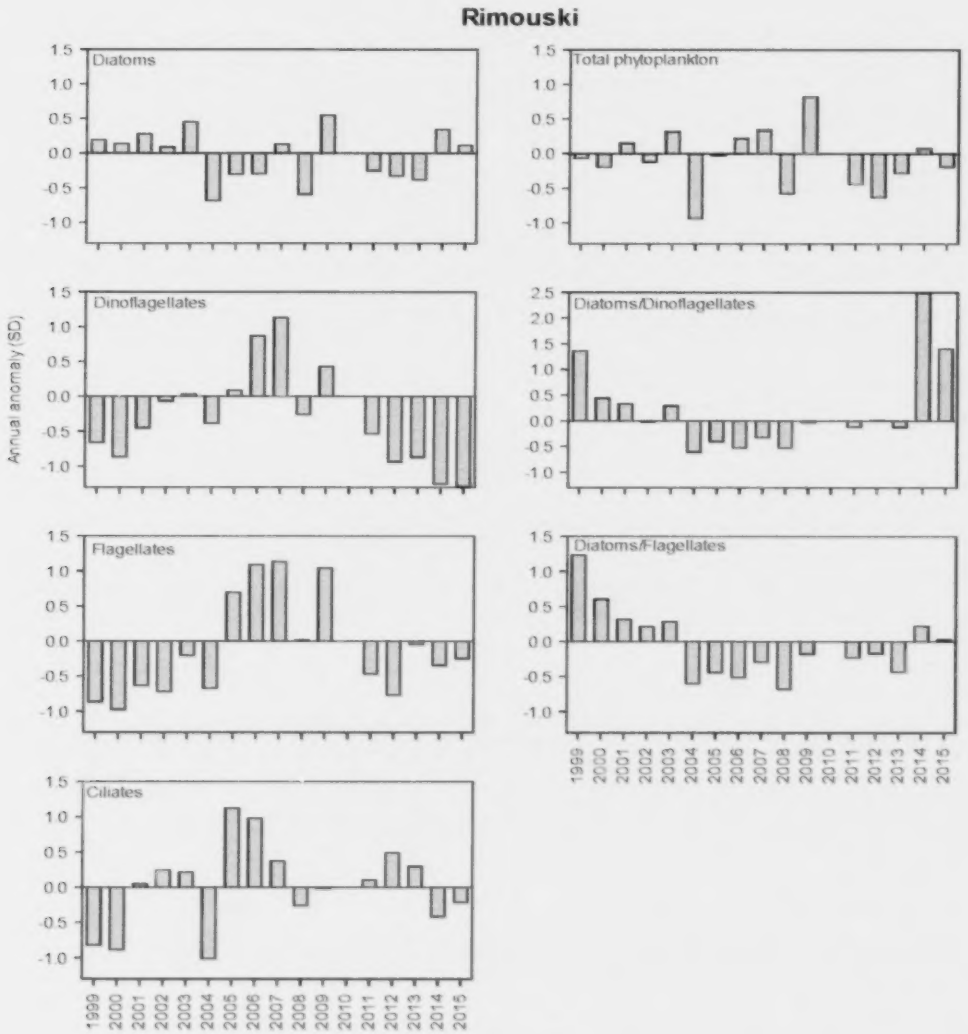

Figure 7. Time series of microplankton abundance anomalies for total phytoplankton and by groups (diatoms, dinoflagellates, flagellates, ciliates) and for the diatom/dinoflagellate and diatom/dinoflagellate ratios at Rimouski station, 1999–2015 (no data for 2010). Note the change in the y-axis scale for the diatom/dinoflagellate ratio.

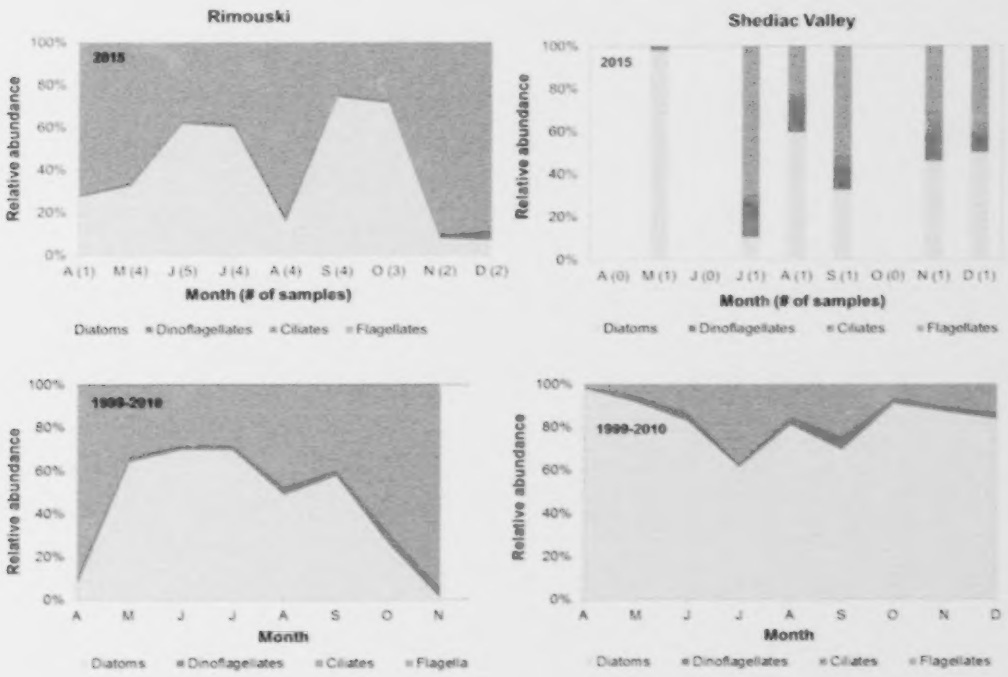

Figure 8. Phytoplankton community composition at Rimouski and Shediac Valley stations for 2015 (top panels) and for the 1999–2010 average (bottom panels). (The ciliate group is shown between the dinoflagellate and flagellate groups on the figures; it is usually so scarce that it is barely visible.)

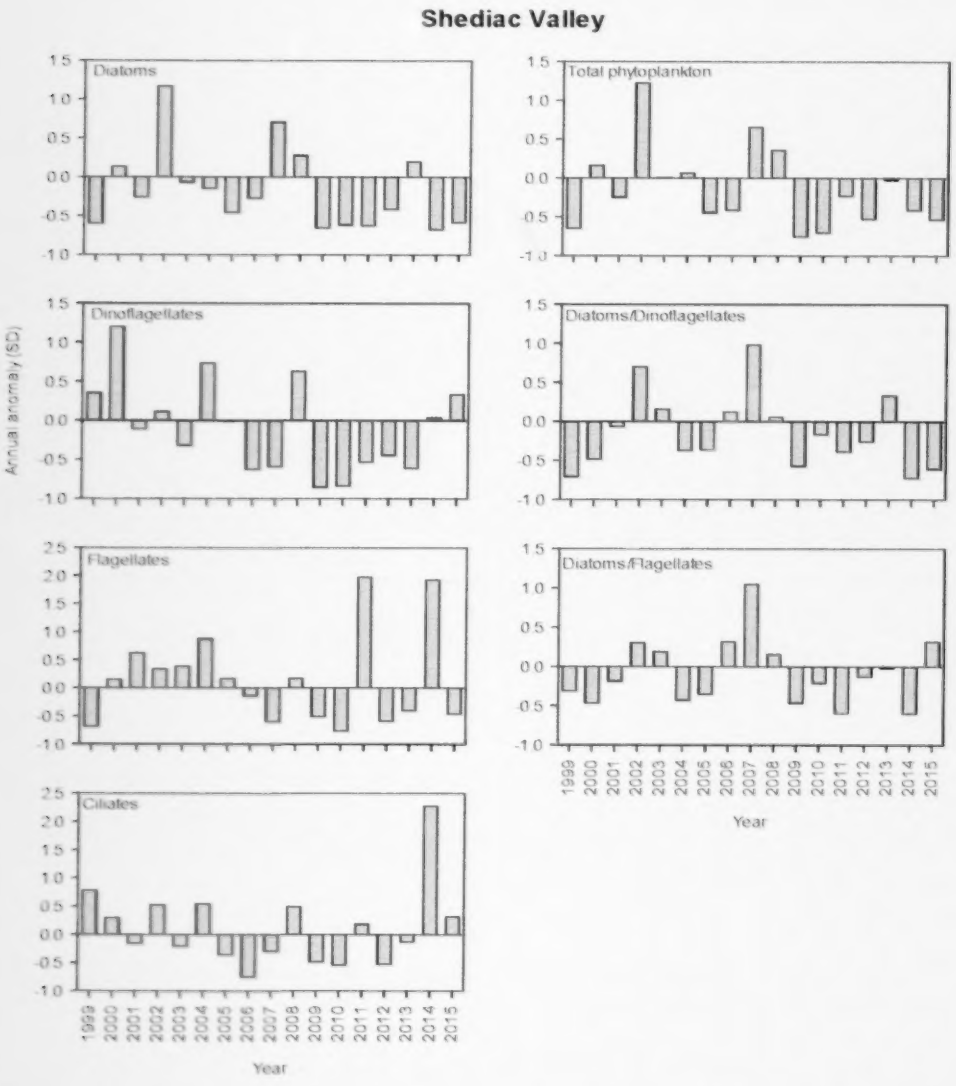

Figure 9. Time series of microplankton abundance anomalies for total phytoplankton and by groups (diatoms, dinoflagellates, flagellates, ciliates), and for the diatom/dinoflagellate and diatom/dinoflagellate ratios at Shediac Valley station, 1999–2015. Note the change in the y-axis scale for flagellates and ciliates.

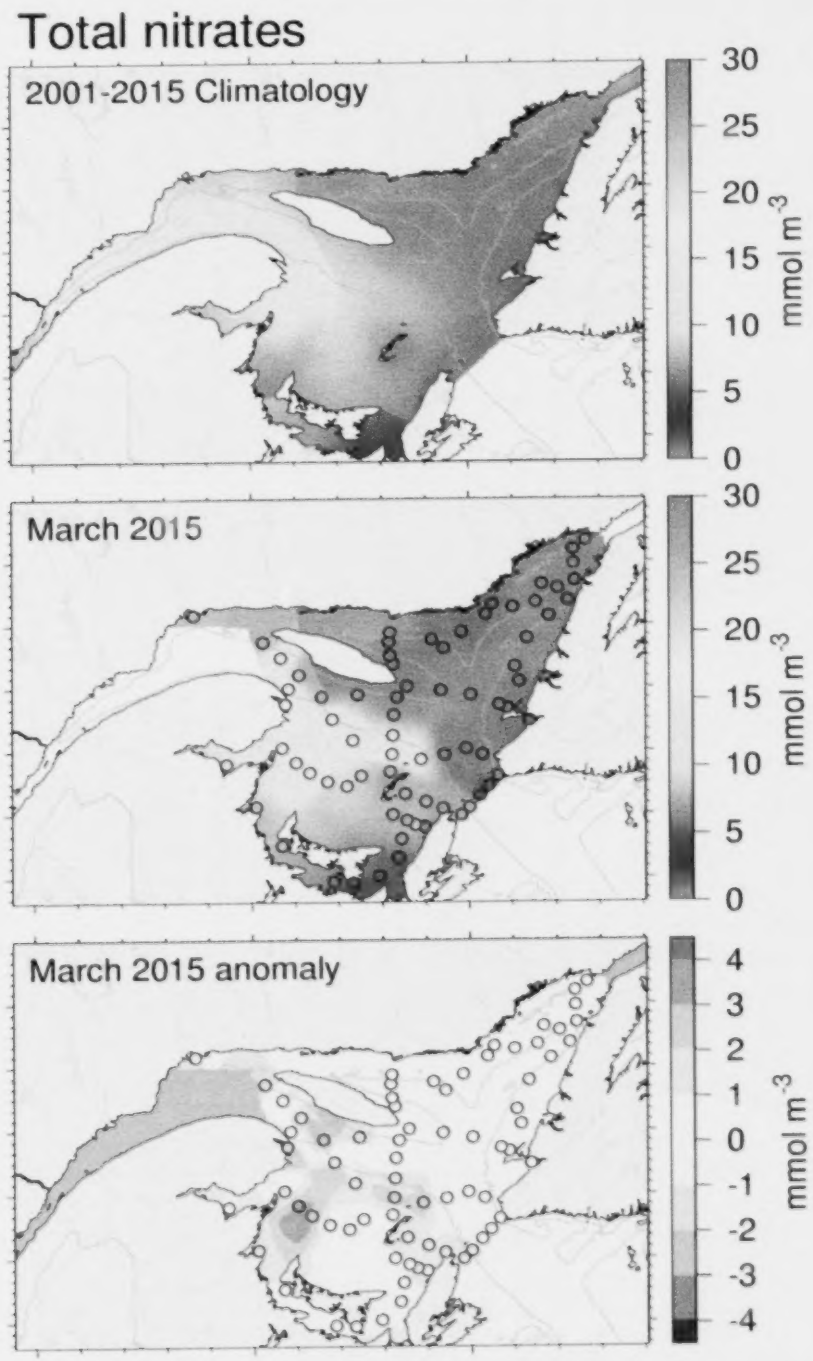

Figure 10. (A) Total nitrate (NO_3^- + NO_2^-) concentrations (mmol m^{-3}) at 2 m collected in the Estuary and Gulf of St. Lawrence during the helicopter survey in late winter (mid-March). (A) 2001–2015 climatology; (B) 3–12 March 2015 (circles indicate sampling locations); (C) 2015 anomalies.

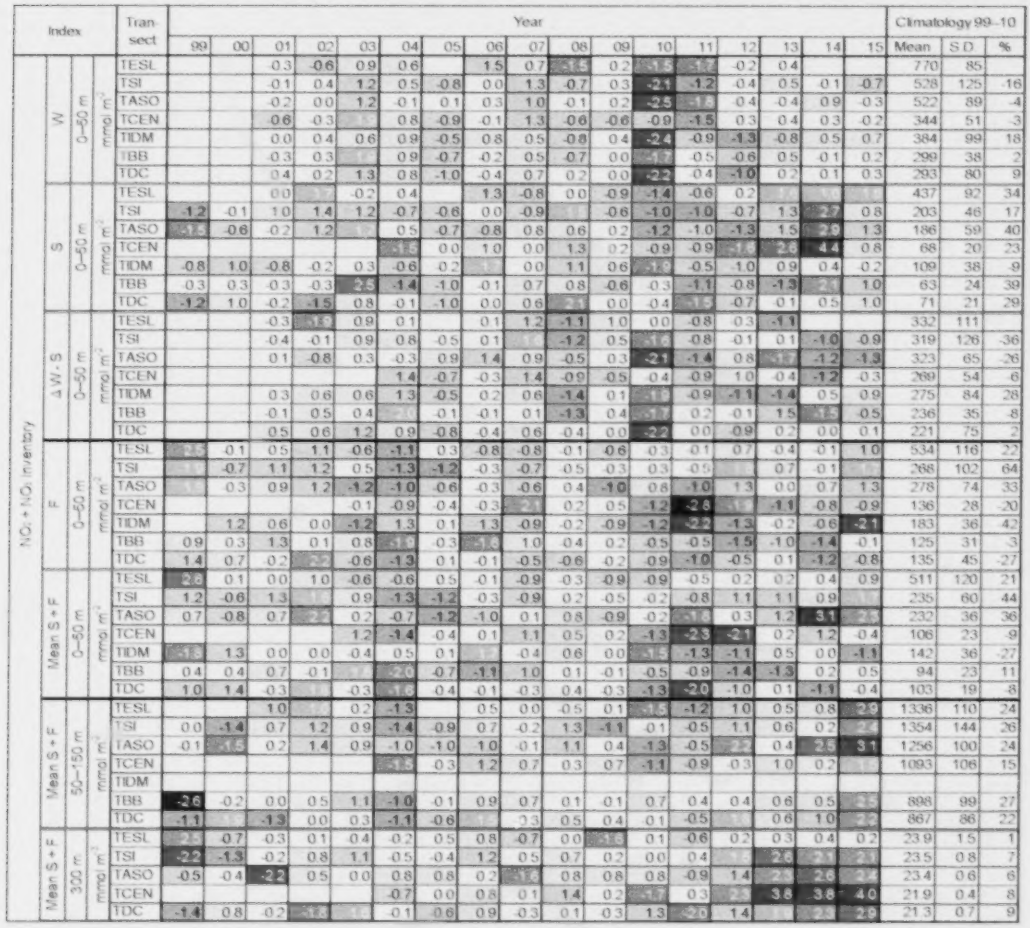
Index
Transect
Year
Climatology 99–10
99 00 01 02 03 04 05 06 07 08 09 10 11 12 13 14 15
Mean S.D %
NO3 + NO2 inventory
W 0–50 m mmol m-2
S 0–50 m mmol m-2
ΔW-S 0–50 m mmol m-2
F 0–50 m mmol m-2
Mean S + F 0–50 m mmol m-2
Mean S + F 50–150 m mmol m-2
Mean S + F 300 m mmol m-2
TESL TSI TASO TCEN TIDM TBB TDC
Chl a concentration
S 0–100m mg m-2
F 0–100m mg m-2
Mean S + F 0–100m mg m-2

Figure 11. Normalized annual anomalies (scorecard) for nutrient inventories and chlorophyll a levels during the winter, late spring, and fall surveys. Blue colours indicate anomalies below the mean and reds are anomalies above the mean. Index W, S, F = winter, spring, and fall, respectively; ΔW – S = difference between winter and spring. Percentages of change in the 2015 values relative to the 1999–2010 climatologies are shown to the right of the table.

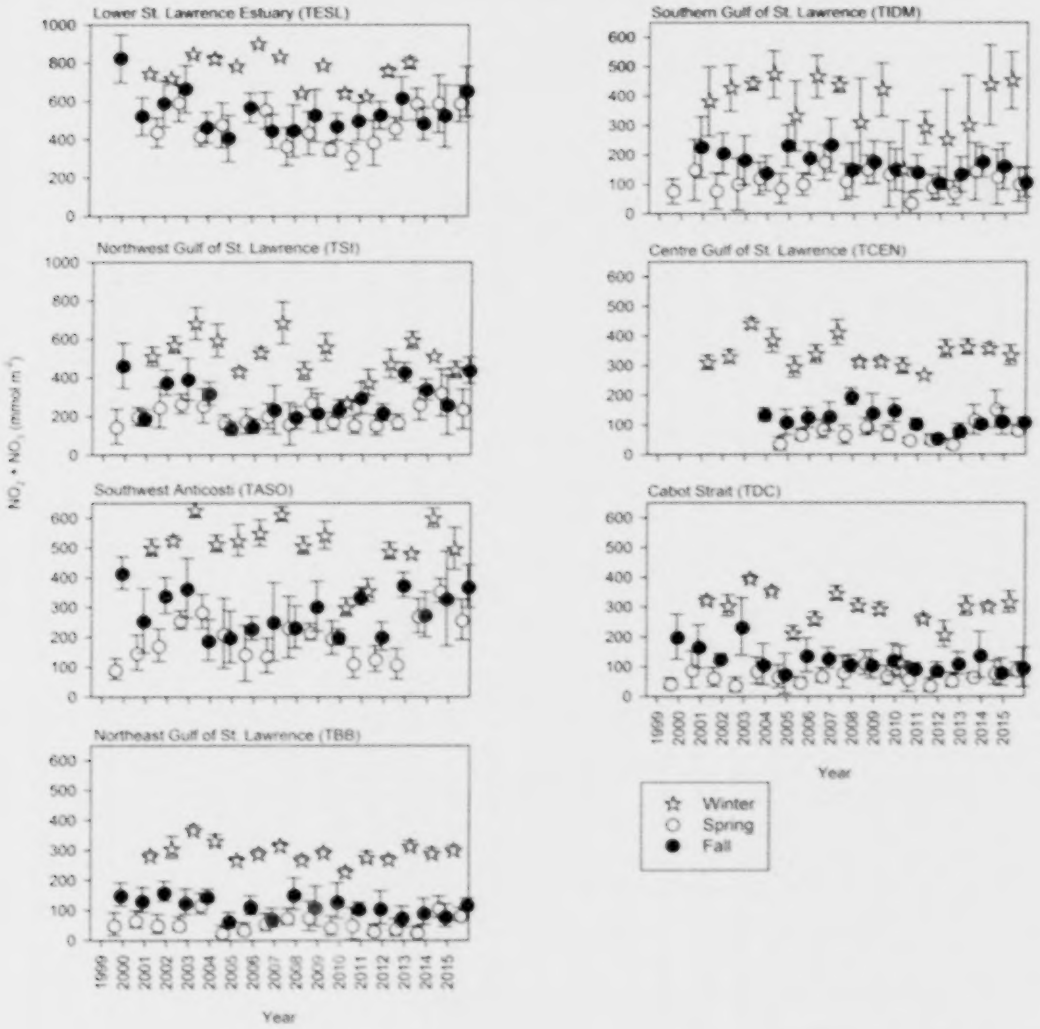

Figure 12. Time series of surface (0–50 m) nitrate inventories along the seven AZMP sections from 1999 to 2015. The late winter inventories were calculated using surface (2 m) concentrations × 50 m (assuming that the nitrate concentrations are homogeneous in the winter mixed layer at that time of the year). Vertical lines represent standard deviations. Note the different scales for the y-axes.

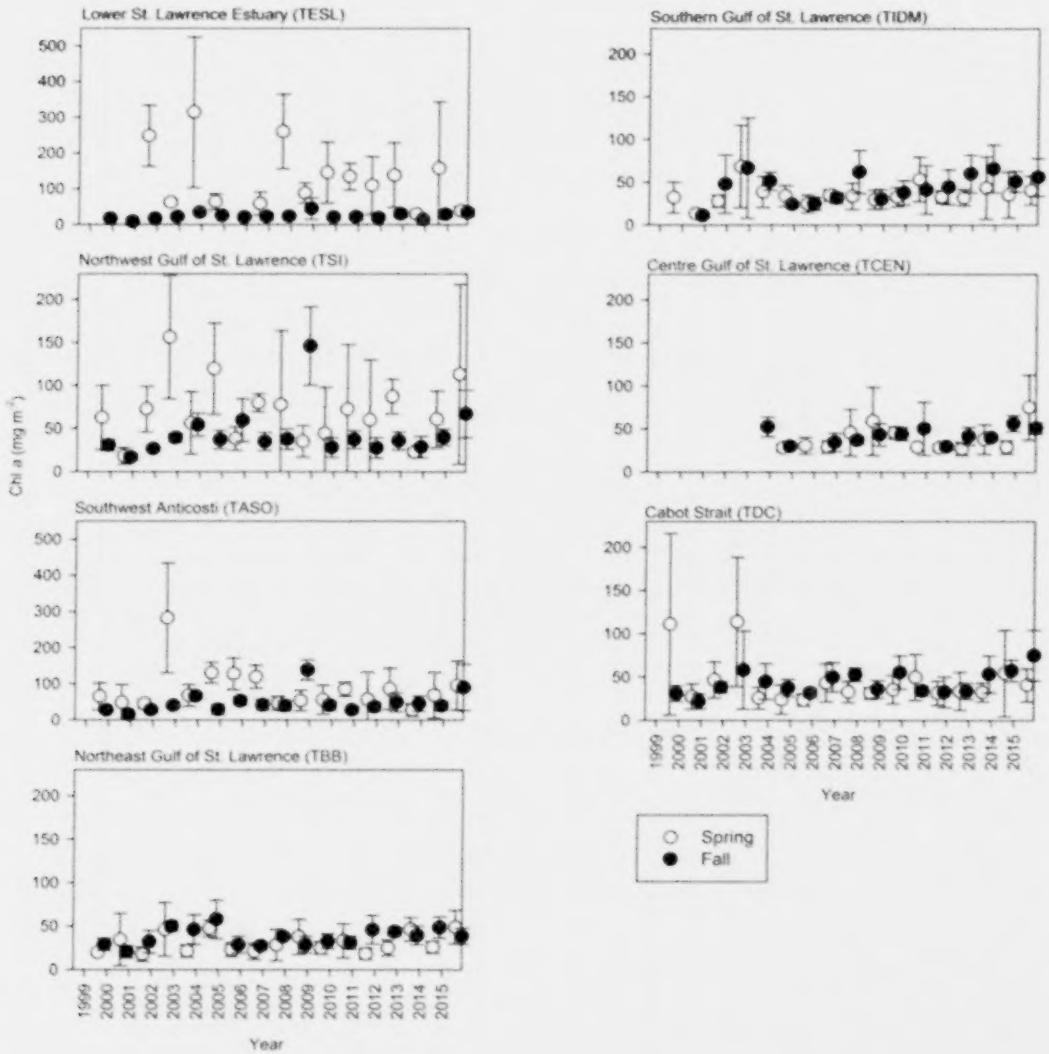

Figure 13. Time series of integrated (0–100 m) chlorophyll a biomass along the seven AZMP sections from 1999–2015. Vertical lines represent standard deviations. Note the different scales for the y-axes.

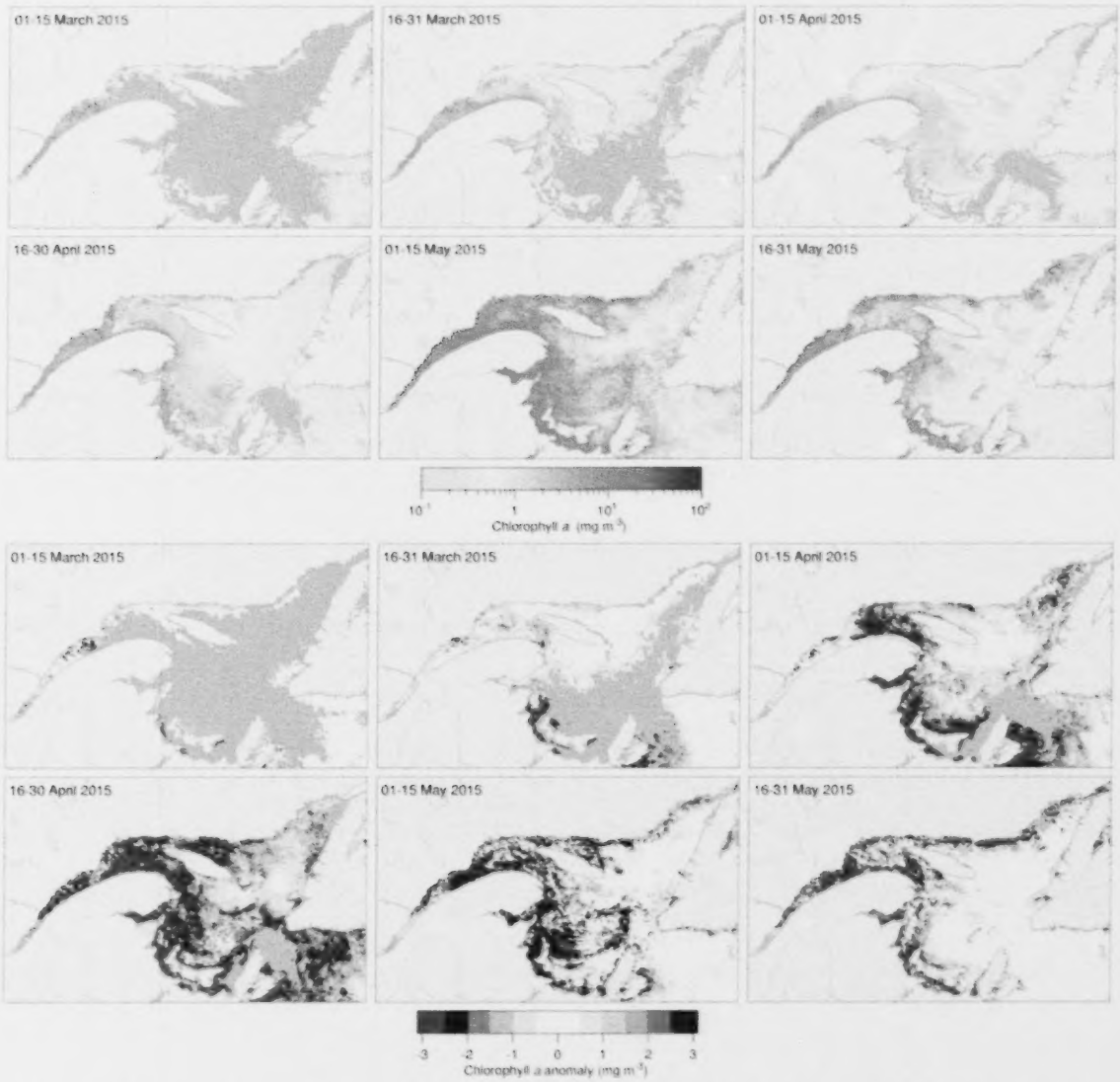

Figure 14. MODIS twice-monthly composite images of surface chlorophyll a (upper panels) and chlorophyll a anomalies (lower panels; based on the 2003–2010 reference period) in the Gulf of St. Lawrence during late winter–early spring 2015.

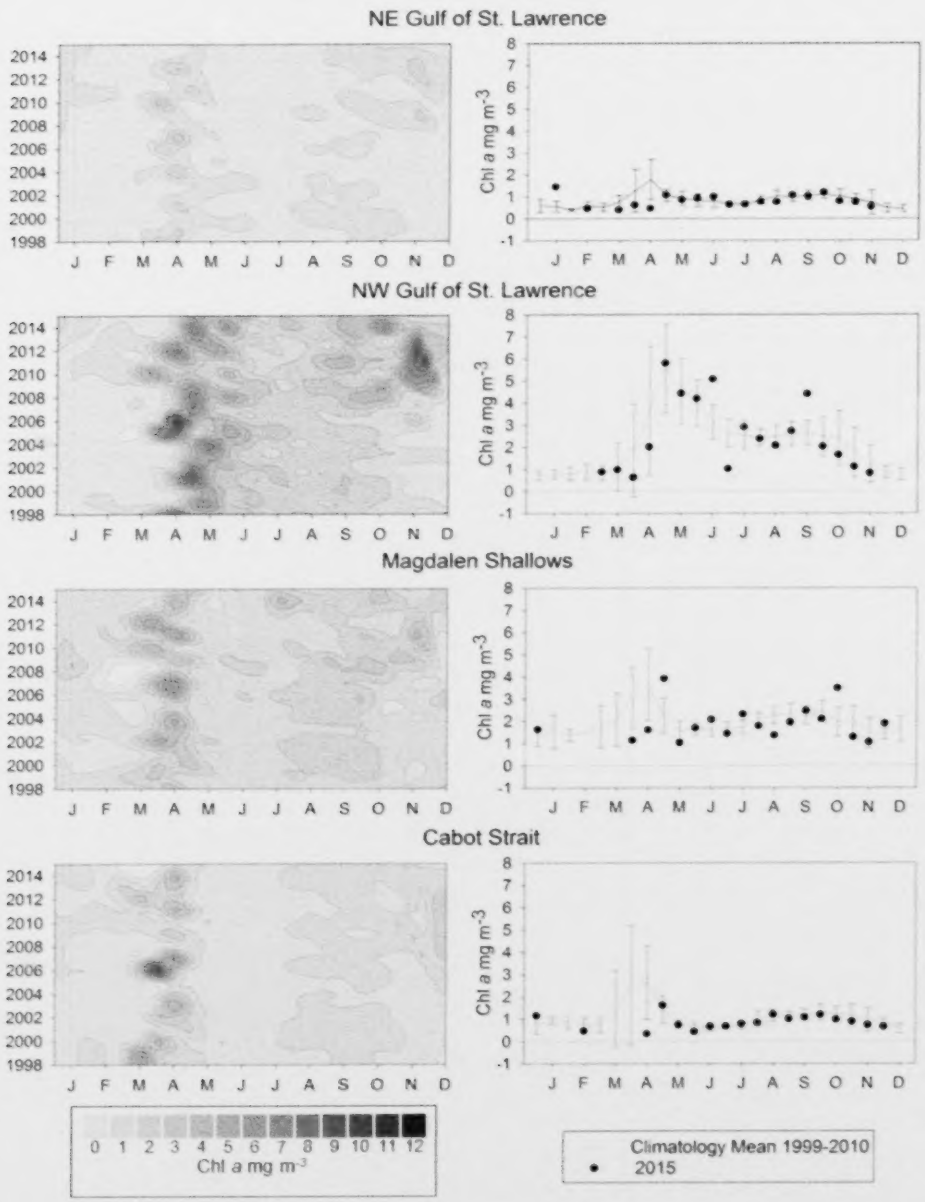
NE Gulf of St. Lawrence
NW Gulf of St. Lawrence
Magdalen Shallows
Cabot Strait
Chl a mg m-3
J F M A M J J A S O N D
0 1 2 3 4 5 6 7 8 9 10 11 12
Chl a mg m-3
Climatology Mean 1999-2010
2015

Figure 15. Left panels: Time series of surface chlorophyll a concentrations from twice-monthly SeaWiFS (1998–2007), MODIS (2008–June 2015), and VIIRS (since July 2015) ocean colour data in the northeast Gulf of St. Lawrence, northwest Gulf of St. Lawrence, Magdalen Shallows, and Cabot Strait statistical subregions (see Fig. 3). Right panels: comparison of 2015 (black circles) surface chlorophyll estimates using satellite ocean colour with mean conditions from 1999–2010 (solid line with standard deviations) for the same statistical subregions.

Indices of change in productivity based on SeaWiFS (1998–2007), MODIS (2008–June 2015), and VIIRS (since July 2015)

Index	Subregion	1998	1999	2000	2001	2002	2003	2004	2005	2006	2007	2008	2009	2010	2011	2012	2013	2014	2015	Mean	S.D.
Mar-Nov Chl a	NEGSL	0.22	0.74	1.12	0.08	-0.75	0.24	0.16	-1.52	0.07	-0.29	-1.57	0.87	1.26	-0.85	-0.81	1.37	-0.95	-1.46	0.95	0.10
	NWGSL	0.82	-0.63	-0.75	0.05	-0.96	-0.92	-0.70	1.33	0.01	-0.91	[illegible]	1.00	0.50	0.01	[illegible]	-0.1	[illegible]	-0.67	2.75	0.40
	MS	-2.10	-1.08	0.38	-1.35	[illegible]	-0.80	-0.03	-1.49	0.58	0.82	0.32	1.20	-0.19	1.25	-0.44	-0.18	1.50	-1.07	2.12	0.20
	CS	0.71	0.46	0.57	-0.60	0.26	0.05	-0.97	-1.41	[illegible]	0.35	-0.86	-0.20	-0.14	-0.28	0.01	0.412	0.44	-1.87	1.19	0.31
Mar-May Chl a	NEGSL	1.36	-0.06	-0.92	0.04	-0.39	-0.81	[illegible]	-1.34	0.48	0.92	-0.61	-0.67	[illegible]	0.32	-0.58	1.268	-1.79	-2.05	1.10	0.20
	NWGSL	[illegible]	-0.26	-1.66	0.86	-0.62	-1.31	0.08	[illegible]	0.74	-0.62	0.27	0.25	0.22	-0.85	1.32	0.143	-0.37	-1.08	3.10	0.63
	MS	-0.74	-0.48	-0.15	-1.07	1.04	0.79	0.86	-1.45	0.07	[illegible]	-1.19	-0.40	0.12	0.69	1.16	-0.38	-0.30	-1.00	2.48	0.57
	CS	1.20	0.86	-0.01	-0.78	-0.03	0.85	-0.71	-1.13	[illegible]	0.78	-1.12	-0.35	-0.56	-0.01	0.51	0.246	0.37	-0.99	1.63	0.75
Jun-Aug Chl a	NEGSL	-1.02	0.58	[illegible]	0.25	-0.46	[illegible]	0.25	-0.43	-0.41	-1.14	-1.54	0.24	-0.73	-1.01	-1.62	-0.16	-1.27	0.03	0.80	0.15
	NWGSL	0.50	-0.55	0.09	-0.61	0.36	-0.51	-0.18	[illegible]	-0.07	-1.35	[illegible]	-0.19	-0.51	-1.64	-1.12	-1.2	1.10	0.12	2.87	0.36
	MS	-1.44	-0.06	0.42	-0.62	0.61	-1.53	0.42	0.10	[illegible]	-0.70	0.62	0.14	-1.51	-1.36	-2.83	-0.66	3.02	-0.40	1.84	0.19
	CS	-0.84	-0.78	[illegible]	0.55	0.54	-0.69	-0.98	[illegible]	0.97	-0.07	-0.47	0.18	0.37	-0.85	-1.85	0.134	0.70	-0.35	0.80	0.13
Sep-Nov Chl a	NEGSL	-0.02	0.69	1.47	-0.07	-0.35	-0.37	-1.43	-1.39	-0.19	-0.64	-0.26	[illegible]	0.74	-0.96	0.54	0.917	1.48	-0.33	0.97	0.19
	NWGSL	-0.70	-0.60	0.09	-0.41	-1.07	-0.17	-0.96	-0.48	-0.61	-0.24	[illegible]	1.46	0.76	[illegible]	[illegible]	0.177	3.42	-0.28	2.32	0.76
	MS	-1.48	-0.90	0.50	-0.35	0.35	-1.07	-0.90	-0.42	-0.26	-0.73	[illegible]	2.07	0.08	1.34	-0.69	0.422	1.02	-0.13	2.10	0.40
	CS	-0.37	-0.70	1.15	-0.40	0.77	-1.03	-1.23	-0.56	[illegible]	-1.31	0.56	0.21	0.90	-0.42	-0.76	0.842	0.98	-1.05	1.20	0.22

Indices of change in spring bloom properties based on SeaWiFS (1998–2007) and MODIS (2008–2015)

Index	Subregion	1998	1999	2000	2001	2002	2003	2004	2005	2006	2007	2008	2009	2010	2011	2012	2013	2014	2015	Mean	S.D.
Start	NEGSL	-0.70	-0.03	[illegible]	0.02	0.24	1.01	-1.10	0.25	-1.11	0.55	0.21	-0.74	-1.47	[illegible]	-0.35	-0.51	[illegible]	0.27	99	9.3
	NWGSL	-0.74	0.59	0.21	-0.46	1.39	0.10	0.76	-0.87	-0.42	0.32	0.53	0.36	-2.53	-0.74	-0.82	-0.09	0.76	-0.84	107	13
	MS	0.37	-0.86	-0.48	0.67	-0.41	0.36	0.99	[illegible]	1.27	-0.25	-6.86	0.73	-2.02	0.43	-1.02	-1.02	1.29	2.11	90	13
	CS	-0.64	-0.83	-0.19	0.60	0.21	0.78	0.63	0.04	-0.54	0.12	[illegible]	-0.09	-2.40	0.54	[illegible]	0.10	0.78	[illegible]	92	14
Duration	NEGSL	-0.39	-0.37	-0.79	-0.28	0.51	[illegible]	0.23	-0.82	-0.06	-0.53	0.12	-0.32	-0.60	-0.99	0.02	-0.25	-0.84	3.35	35	22
	NWGSL	-0.12	0.48	[illegible]	0.43	-1.24	1.35	0.48	-0.85	-0.74	-0.01	-0.60	-0.95	-0.41	0.16	-0.68	0.93	-0.79	3.00	42	22
	MS	-0.11	-0.49	[illegible]	-0.71	0.23	0.05	-1.32	-2.23	-1.24	0.72	-2.23	-0.02	0.86	-0.13	-0.22	0.94	-1.10	-1.38	37	16
	CS	0.09	-0.55	-1.23	0.93	-1.24	-1.34	0.13	0.54	0.28	0.57	-0.70	0.88	[illegible]	-0.49	[illegible]	0.17	-1.29	-0.52	30	12
Magnitude	NEGSL	[illegible]	-0.56	-1.23	0.29	-0.30	1.37	0.71	-1.43	0.75	1.17	-0.70	-1.08	1.00	-0.98	-0.37	0.82	-1.53	0.66	39	18
	NWGSL	0.80	0.22	1.34	0.69	-1.49	1.13	1.35	-0.73	-0.27	0.45	-0.61	-0.91	-1.16	-1.11	0.57	0.78	-0.66	4.33	156	51
	MS	-0.10	-0.91	-0.26	-0.66	0.59	0.75	-1.05	-1.64	-0.87	[illegible]	-1.84	-0.45	0.87	0.61	1.48	-0.56	-0.29	-0.99	81	49
	CS	-2.57	0.41	-0.37	-0.34	0.06	-0.18	-0.45	-0.98	-2.45	1.31	-1.24	-0.11	-0.52	-0.03	[illegible]	-0.30	-0.11	-1.08	67	42
Amplitude	NEGSL	[illegible]	-0.27	-0.41	0.39	-0.78	-0.91	0.03	-0.65	0.40	[illegible]	-0.81	-0.81	[illegible]	0.55	-0.51	0.79	-0.88	-1.16	1.79	0.97
	NWGSL	0.82	-0.90	-1.50	-0.39	1.23	-1.19	0.19	0.91	1.27	0.14	0.18	1.01	-1.13	[illegible]	2.80	-0.94	0.78	-0.61	5.94	1.50
	MS	-0.03	-1.15	-1.45	-0.33	0.61	1.13	-0.32	-2.64	0.17	[illegible]	-2.64	-0.70	0.27	1.20	[illegible]	-1.42	[illegible]	0.11	3.16	1.20
	CS	[illegible]	0.65	0.46	-0.79	1.24	1.00	-0.64	-1.15	[illegible]	0.48	-1.16	-0.63	-1.93	0.10	[illegible]	-0.53	1.02	-1.91	3.65	2.32

Figure 16. Annual anomalies (scorecard) of productivity indices (upper section; mean surface chlorophyll for various time periods; mg m^{-3}) and indices of change of spring bloom properties (lower section) across the Gulf of St. Lawrence statistical subregions from 1998 to 2015. The spring bloom indices are start (day of the year), duration (days), magnitude (mg chl m^{-2}), and amplitude (mg chl m^{-3}). The reference period used to compute annual anomalies was 1999–2010. Subregions are northeast and northwest GSL, Magdalen Shallows, and Cabot Strait (see Fig. 3). Blue colours indicate anomalies below the mean and reds are anomalies above the mean. The climatological means and standard deviations are shown to the right of the table.

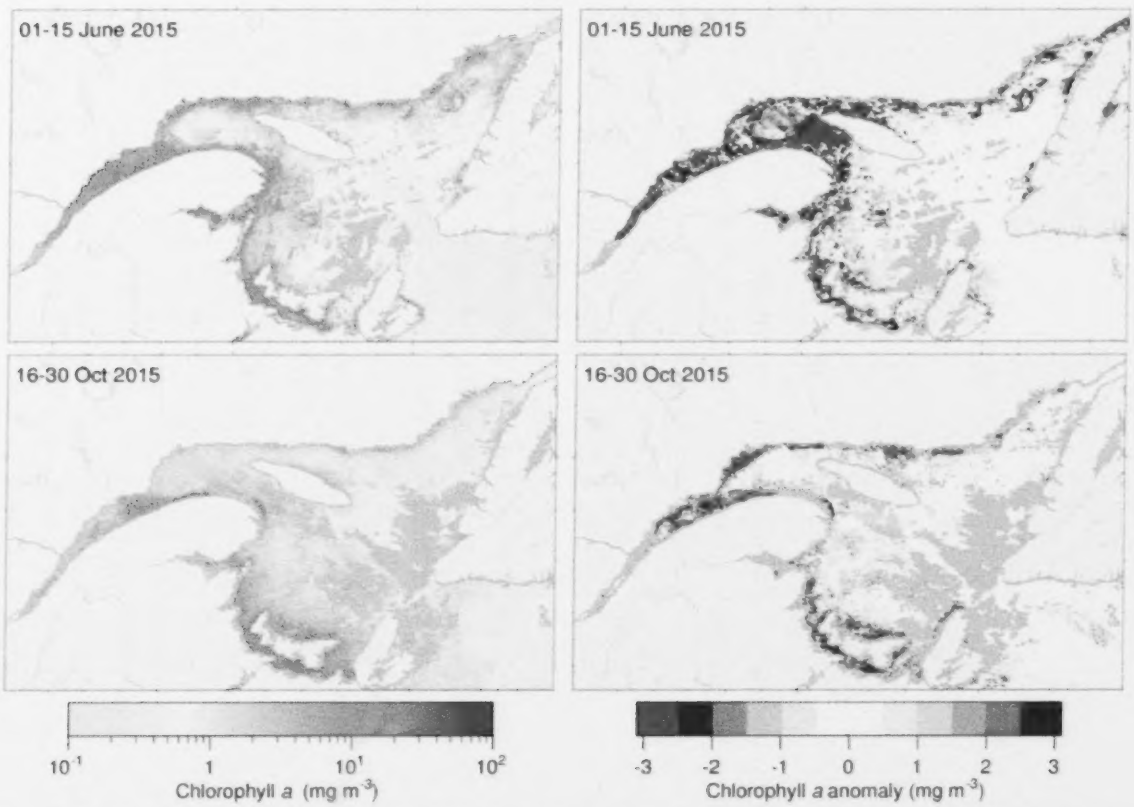

Figure 17. MODIS and VIIRS composite images of surface chlorophyll a (left) and chlorophyll a anomaly (right; based on the 2003–2010 reference period) in the Gulf of St. Lawrence. The images' date intervals (MODIS 1–15 June and VIIRS 16–31 Oct. 2015) coincide with those of the late spring (31 May – 19 June 2015) and fall (19 Oct. – 6 Nov. 2015) surveys.

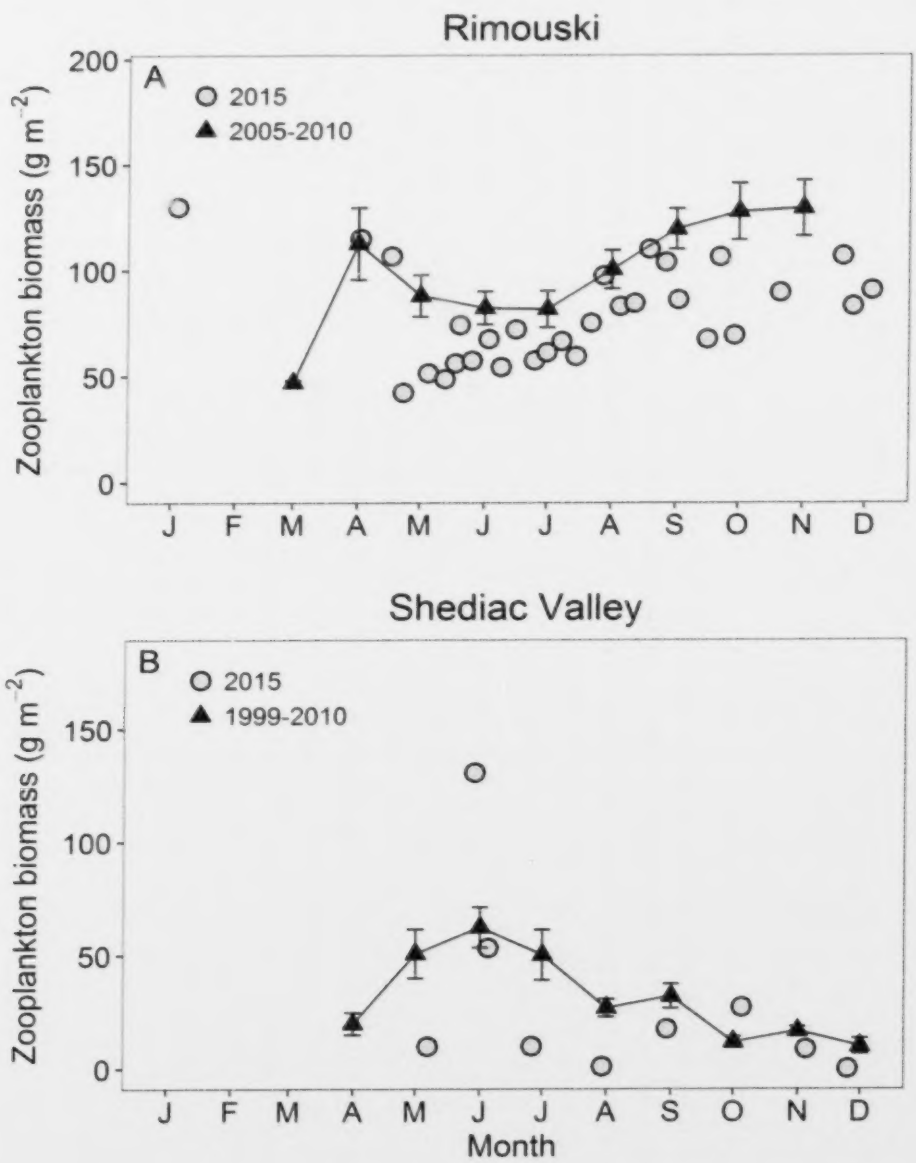

Figure 18. Comparison of total zooplankton biomass in 2015 (circles) with the monthly climatology from (A) Rimouski (2005–2010) and (B) Shediac Valley (1999–2010) stations (triangles with solid line). Vertical lines are standard errors of the monthly means.

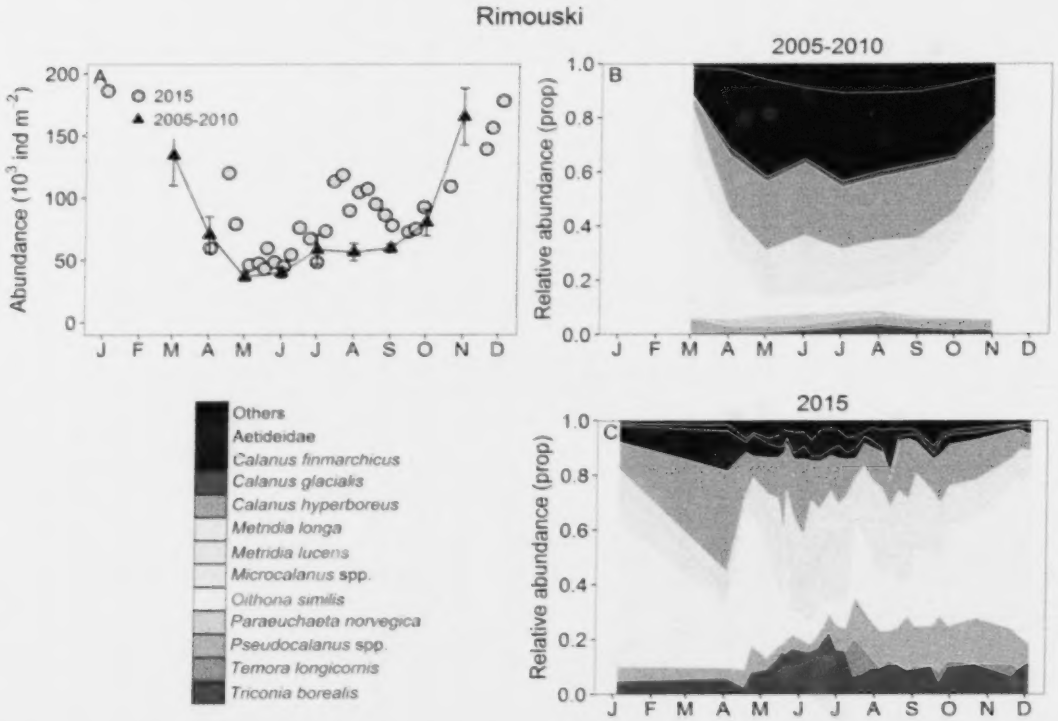

Figure 19. Seasonal variability of dominant copepods at Rimouski station. Copepod abundance (excluding nauplii) during the reference period (triangles and solid line with standard errors) and 2015 (circles) (A); climatology of the relative abundance of the top 95% of identified copepod taxa during the 2005–2010 period (B) and in 2015 (C). While Calanus glacialis *and* Paraeuchaeta norvegica *appear in the climatology, they were no longer in the top 95% in 2015, being replaced by the Aetideidae group and* Metridia lucens.

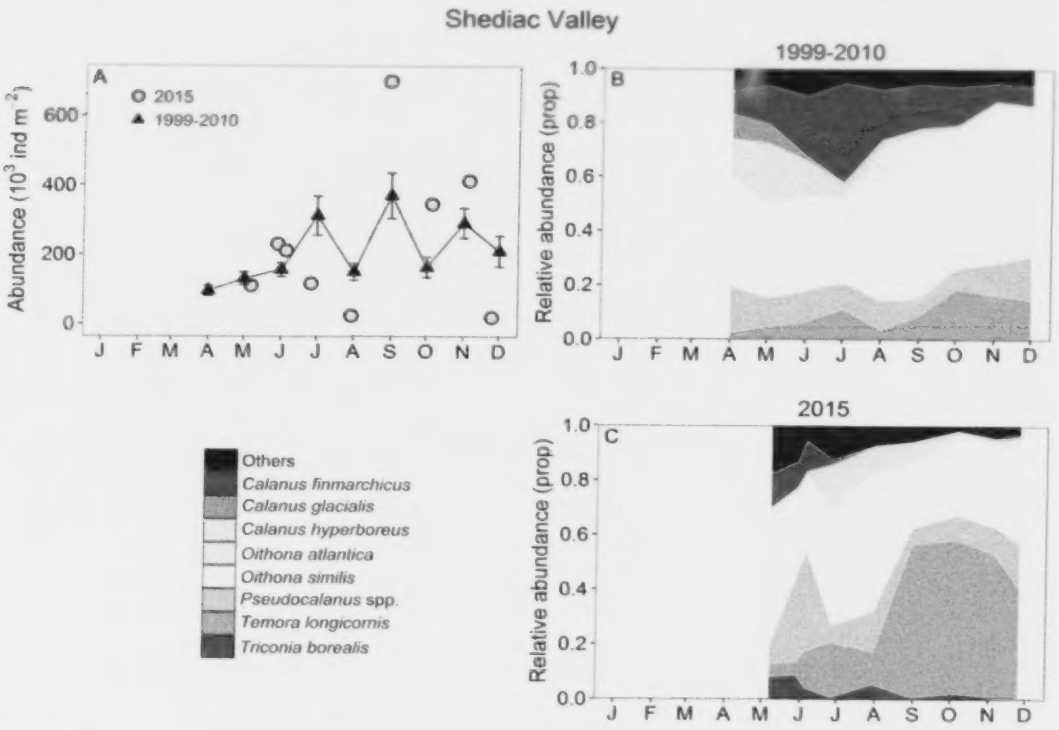

Figure 20. Seasonal variability of dominant copepods at Shediac Valley station. Copepod abundance (excluding nauplii) during the reference period (triangles and solid line with standard errors) and 2015 (circles) (A); climatology of the relative abundance of the top 95% of identified copepod taxa during the 1999–2010 period (B) and in 2015 (C). In 2015, Calanus glacialis *and* Calanus hyperboreus *were replaced by* Triconia borealis *and* Oithona atlantica.

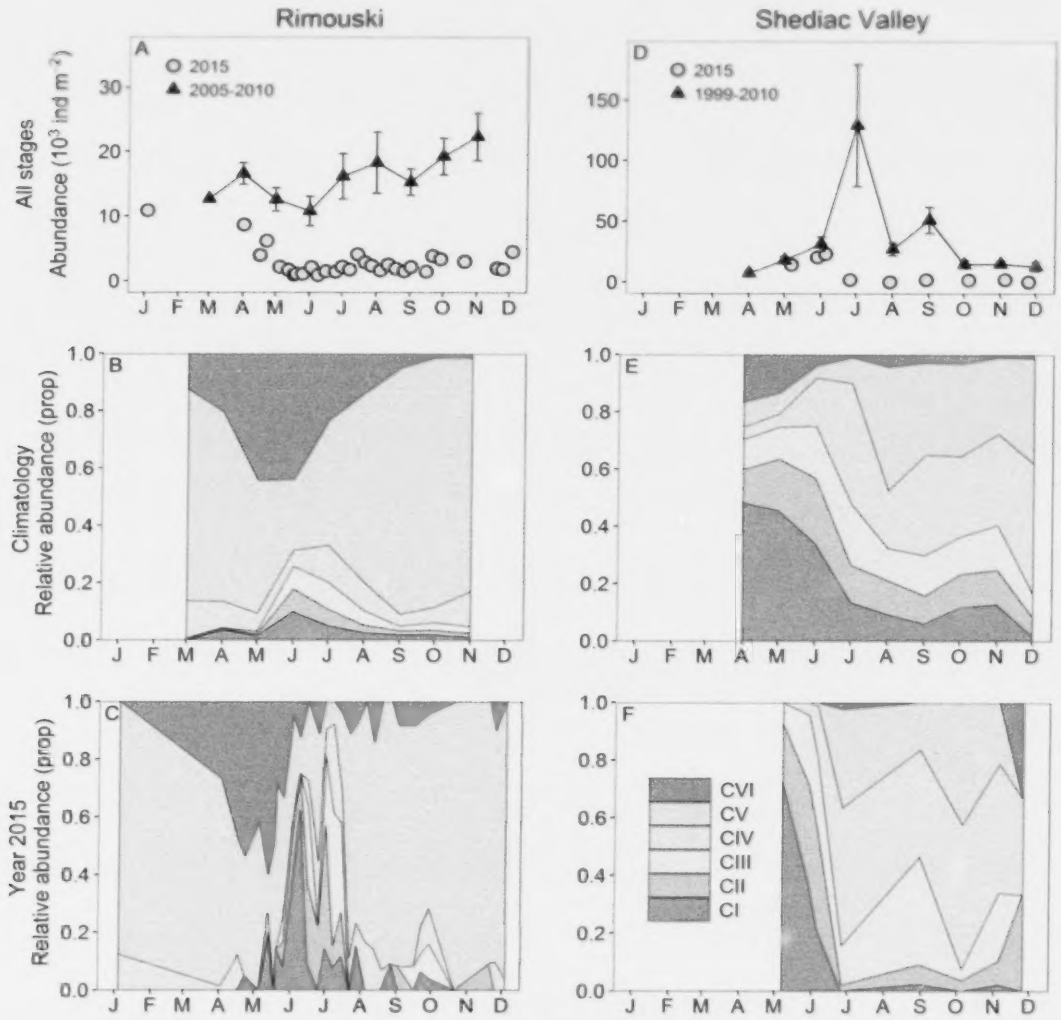

Figure 21. Seasonal variability in Calanus finmarchicus *copepodite abundance at Rimouski (A–C) and Shediac Valley (D–F) stations. The climatologies of the combined counts for the reference periods (triangles and solid lines with standard errors) are plotted with data from 2015 (circles) (A, D). The seasonal variabilities for the individual copepodite stages for the reference periods (B, E) and for 2015 (C, F) are also shown.*

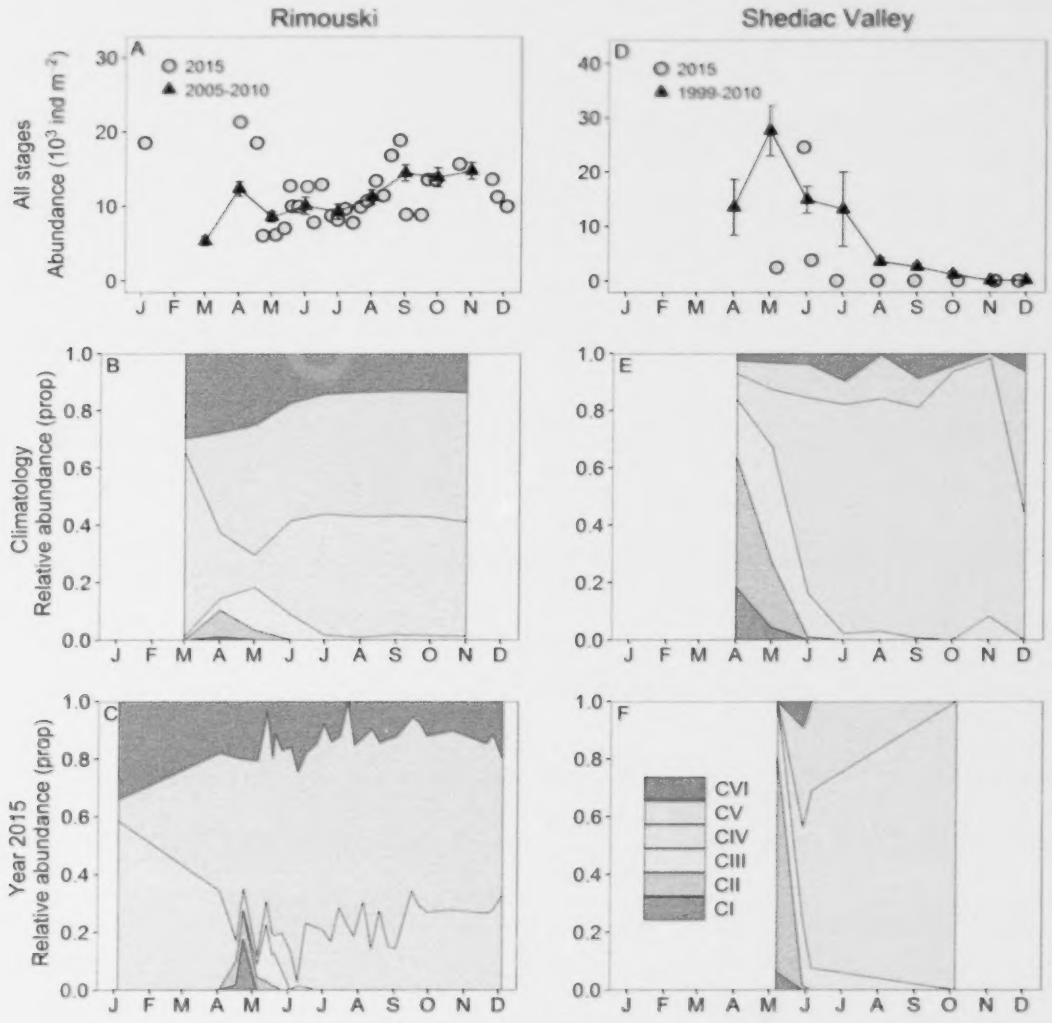

Figure 22. Seasonal variability in Calanus hyperboreus *copepodite abundance at Rimouski (A–C) and Shediac Valley (D–F) stations. The climatologies of the combined counts for the reference periods (triangles and solid lines with standard errors) are plotted with data from 2015 (circles) (A, D). The seasonal variabilities for the individual copepodite stages for the reference periods (B, E) and for 2015 (C, F) are also shown.*

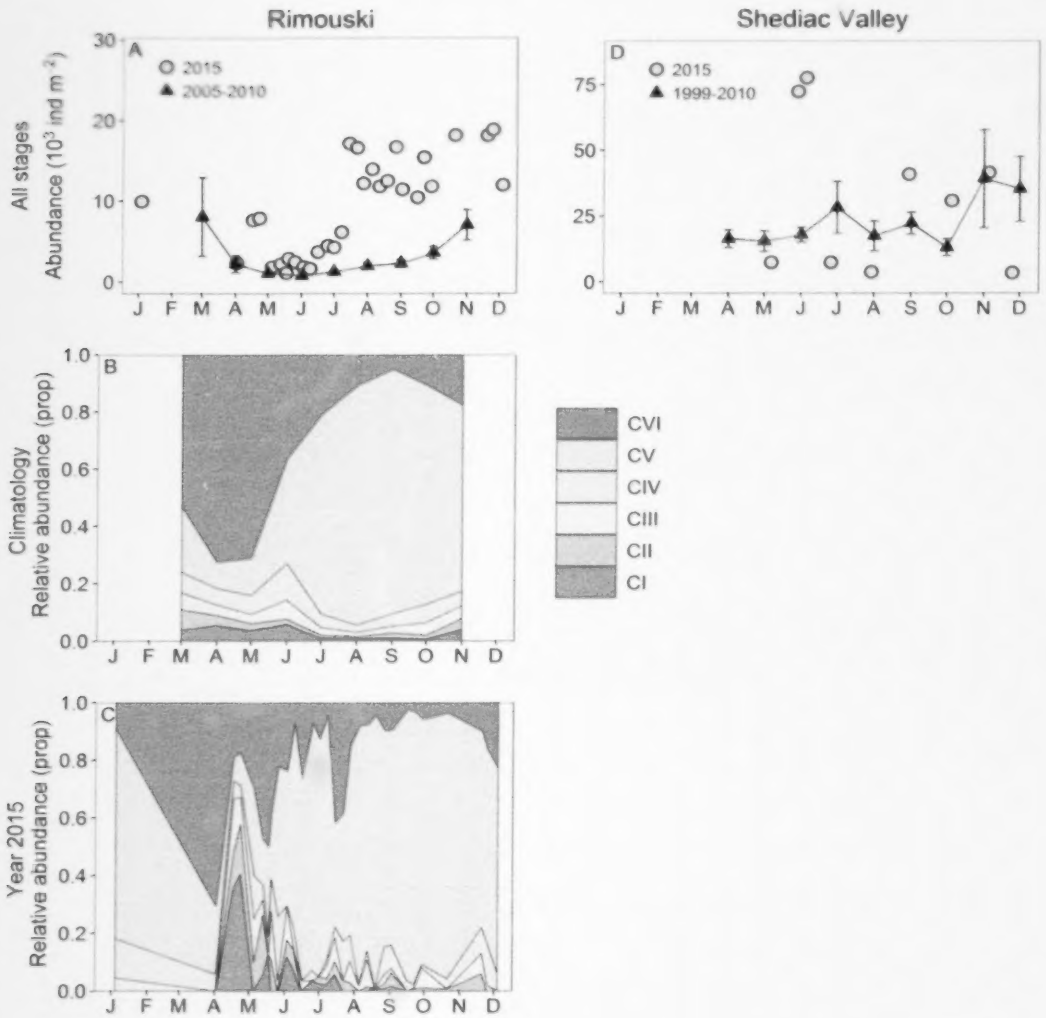

Figure 23. Seasonal variability in Pseudocalanus *spp. copepodite abundance at Rimouski (A–C) and Shediac Valley (D) stations. The climatologies of the combined counts for the reference periods (triangles and solid lines with standard errors) are plotted with data from 2015 (circles) (A, D). Seasonal variability for the individual copepodite stages for the reference period (B) and for 2015 (C) are also shown. No stage information is available for Shediac Valley.*

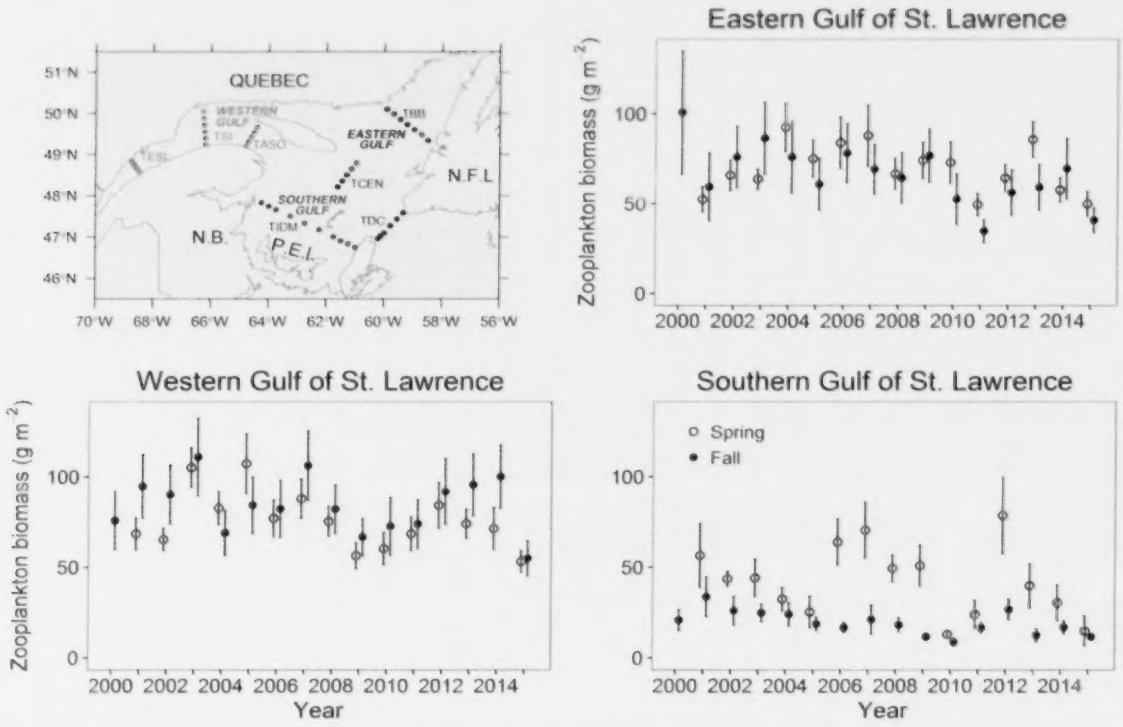

Figure 24. Mean total zooplankton biomass during spring (open circles) and fall (filled circles) for the three subregions of the Estuary and Gulf of St. Lawrence from 2000 to 2015. Vertical lines represent standard errors.

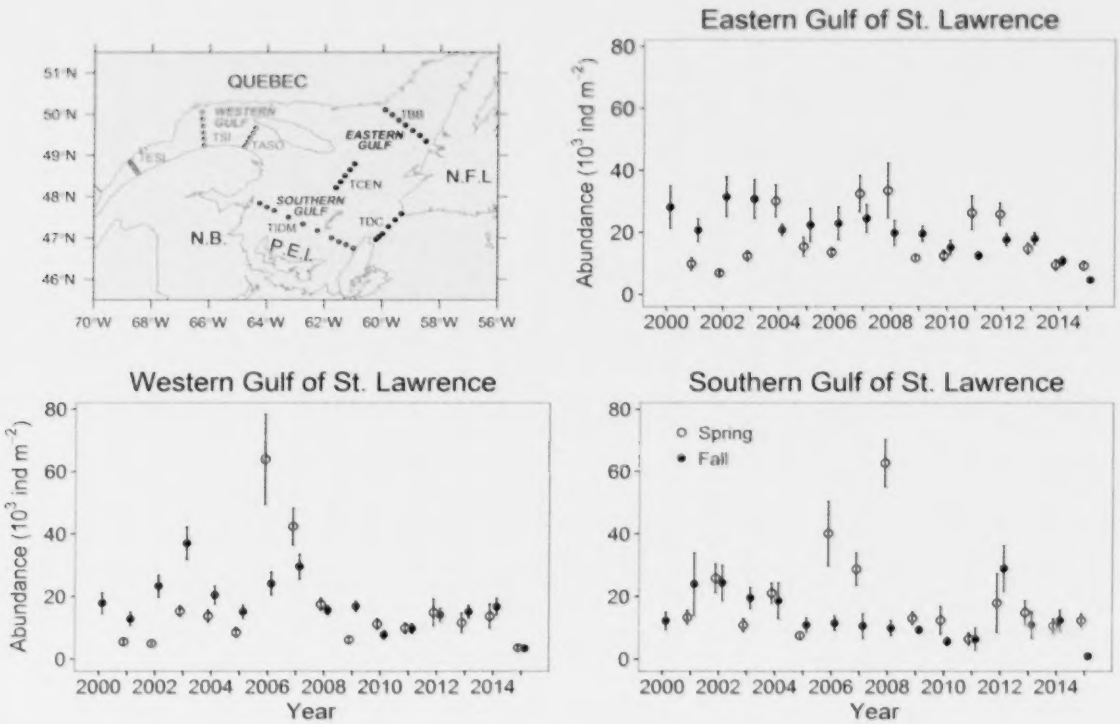

Figure 25. Mean total abundance of Calanus finmarchicus *during spring (open circles) and fall (filled circles) for the three subregions of the Estuary and Gulf of St. Lawrence from 2000 to 2015. Vertical lines represent standard errors.*

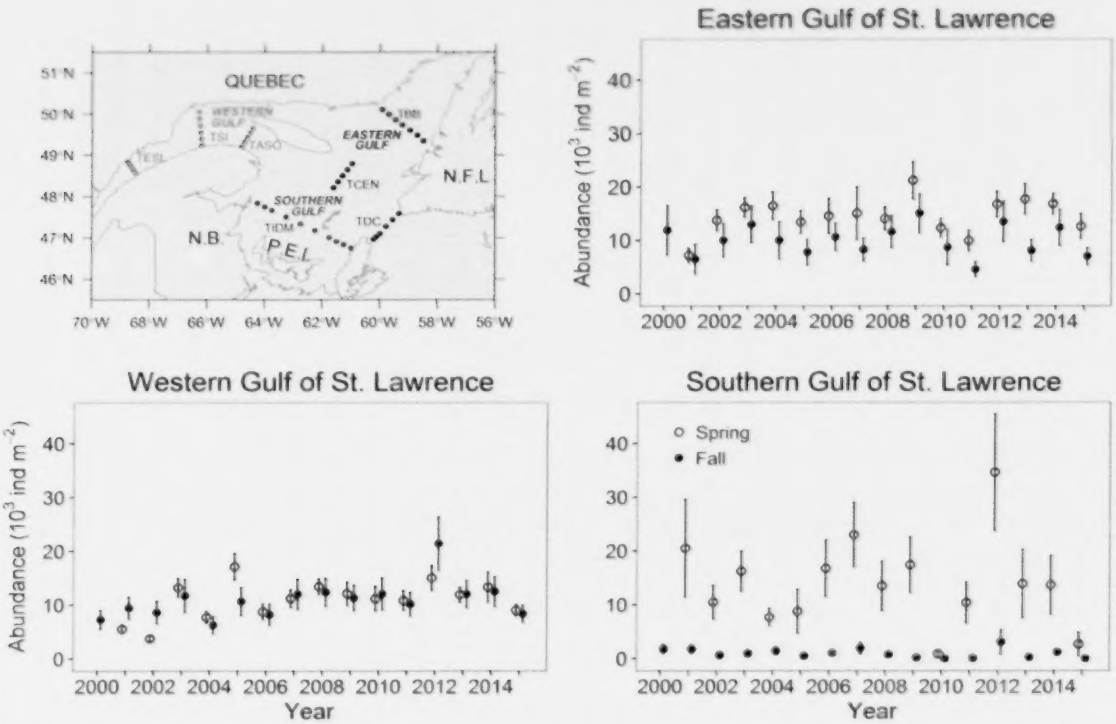

Figure 26. Mean total abundance of Calanus hyperboreus *during spring (open circles) and fall (filled circles) for the three subregions of the Estuary and Gulf of St. Lawrence from 2000 to 2015. Vertical lines represent standard errors.*

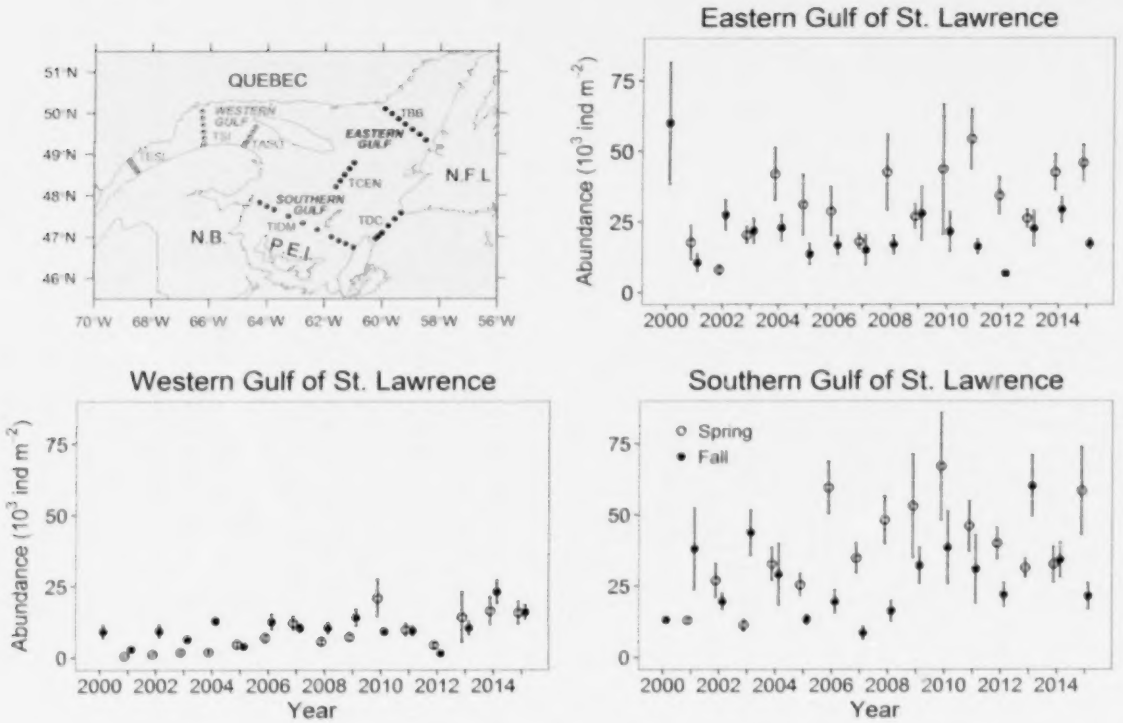

Figure 27. Mean total abundance of Pseudocalanus *spp. during spring (open circles) and fall (filled circles) for the three subregions of the Estuary and Gulf of St. Lawrence from 2000 to 2015. Vertical lines represent standard errors.*

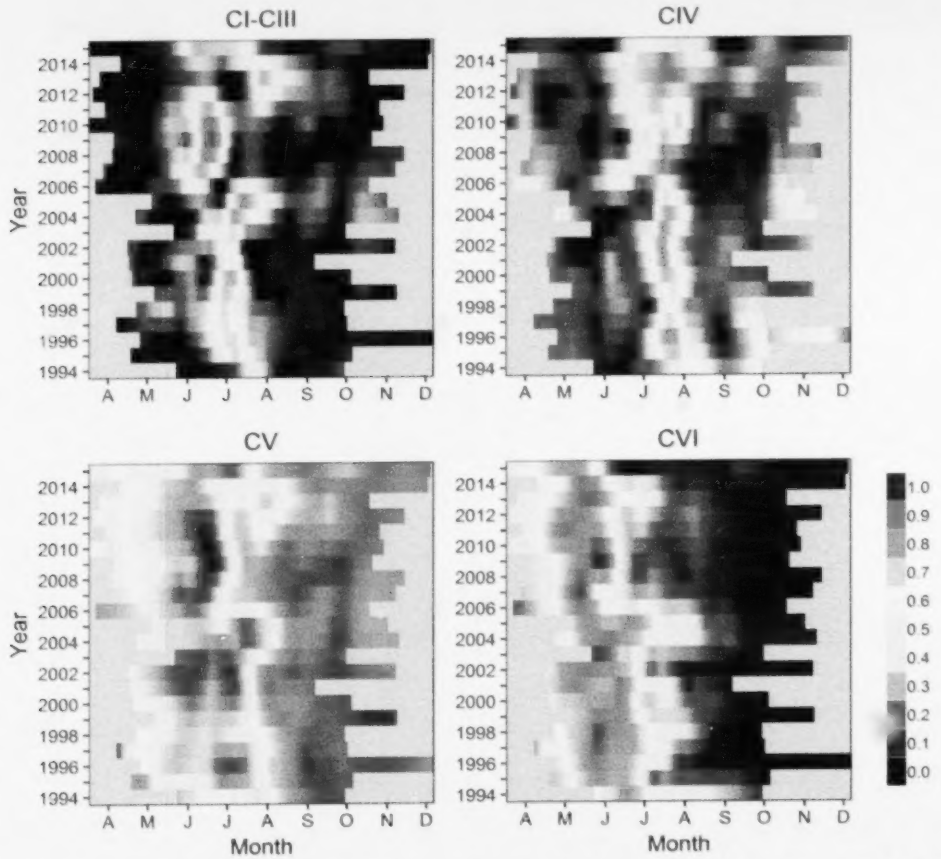

Figure 28. Seasonal cycle in relative proportions of total abundance for stages CI–CIII, CIV, CV, and CVI (male+female) Calanus finmarchicus *copepodites from 1994 to 2015 at Rimouski station. Proportions are normalized by the annual maximum and smoothed using Loess.*

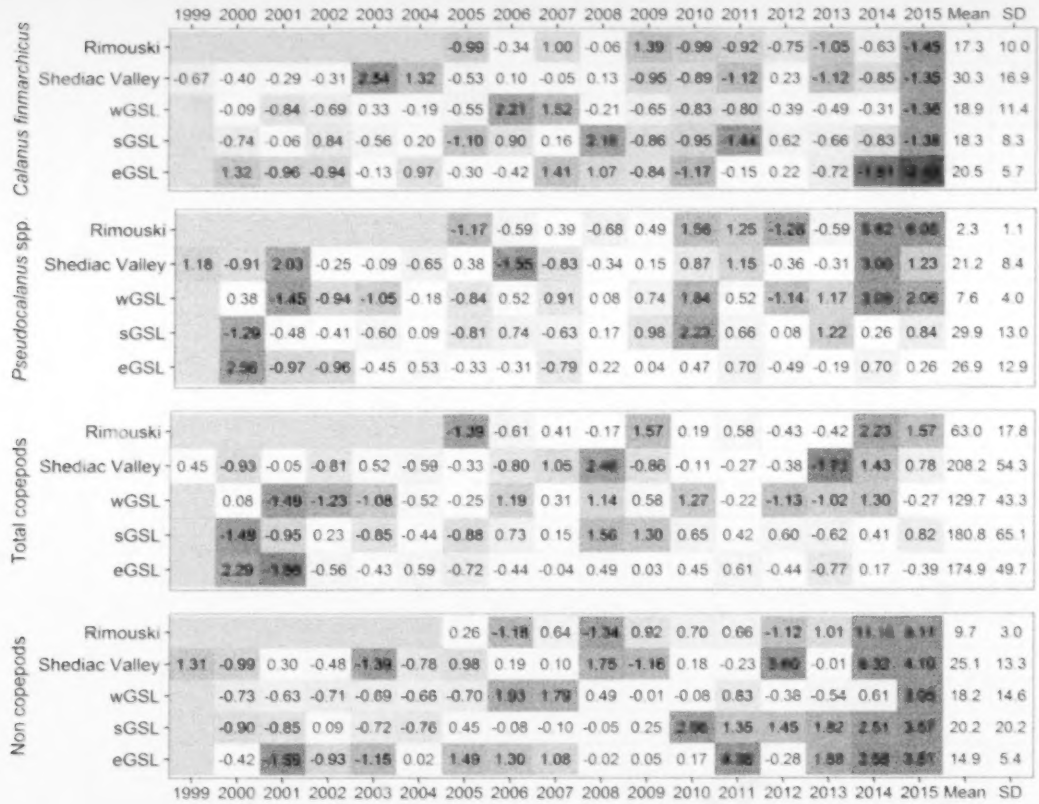

Figure 29. Normalized annual anomalies (scorecard) for four zooplankton categories at the high-frequency monitoring sites and the three subregions of the Estuary and Gulf of St. Lawrence (reference period: 1999–2010 [2005–2010 for Rimouski]). Blue colours indicate anomalies below the mean and reds are anomalies above the mean. The climatological means and standard deviations are also given (abundance; $\times 10^3$ ind. m^{-2}).

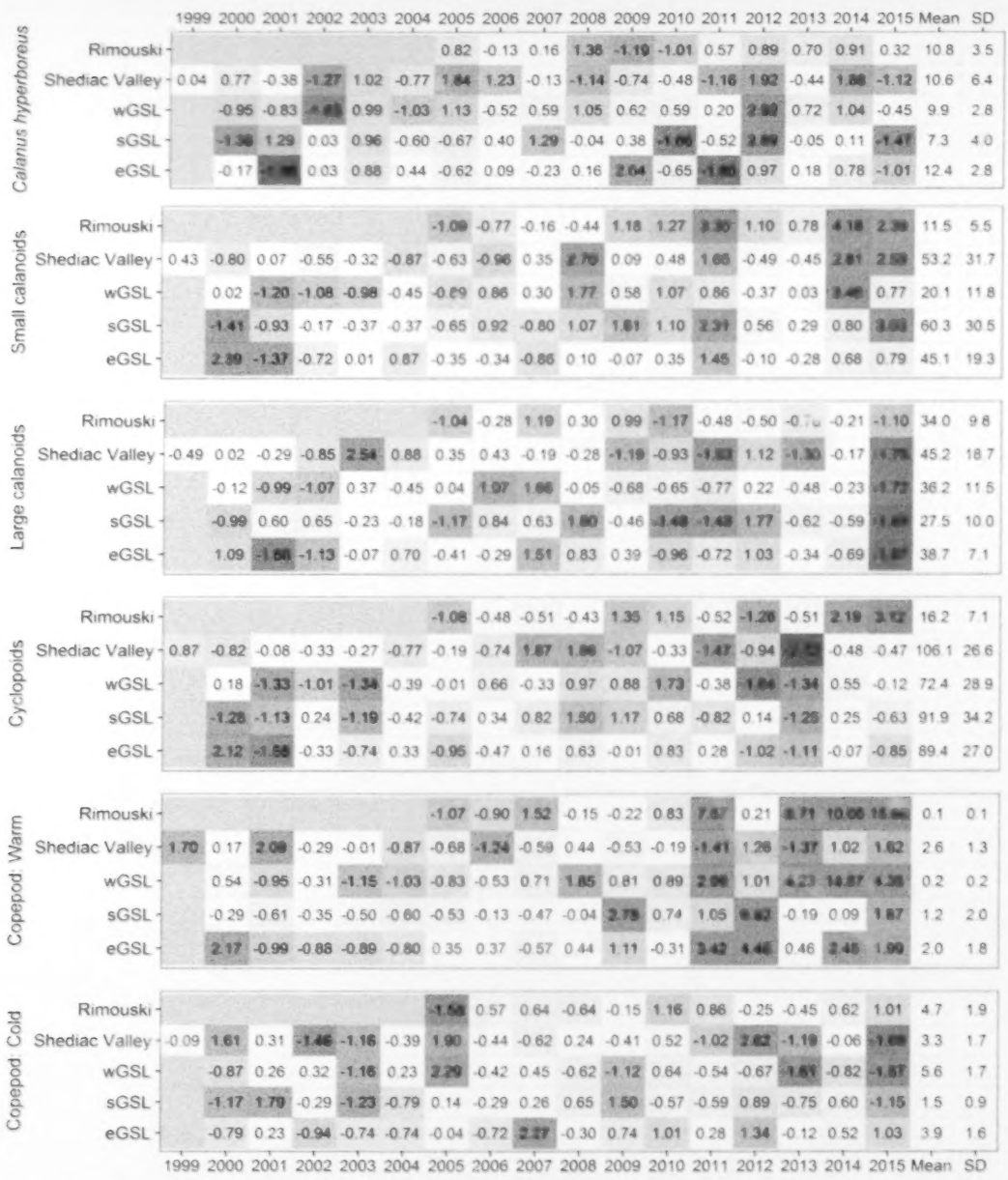

Figure 30. Normalized annual anomalies (scorecard) for six categories of zooplankton assemblages at the high-frequency monitoring sites and the three subregions of the Estuary and Gulf of St. Lawrence (reference period: 1999–2010 [2005–2010 for Rimouski station]). Blue colours indicate anomalies below the mean and reds are anomalies above the mean. The climatological means and standard deviations are also given (abundance; $\times 10^3$ ind. m^{-2}). Small calanoids: mostly neritic species such as Pseudocalanus *spp.*, Acartia *spp.*, Temora longicornis, *and* Centropages *spp.; large calanoids: mostly* Calanus *and* Metridia *species; cyclopoids: mostly* Oithona *spp. and* Triconia *spp.; warm-water species:* Metridia lucens, Centropages *spp.*, Paracalanus *spp., and* Clausocalanus *spp.; and cold/arctic species:* Calanus glacialis *and* Metridia longa.

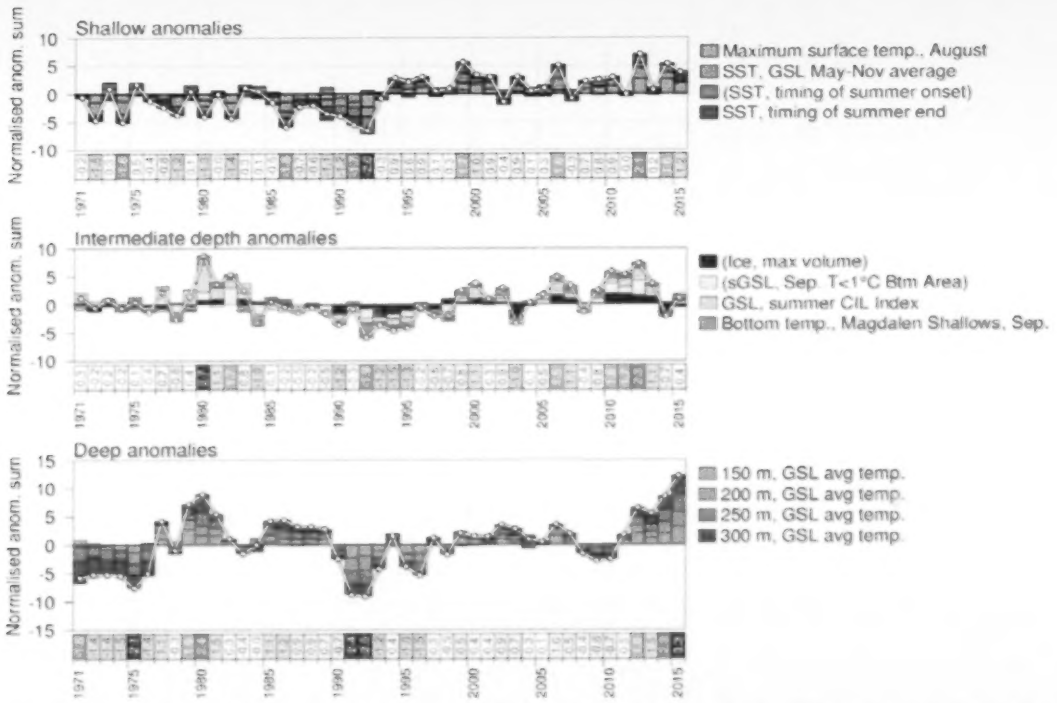

Figure 31. Composite climate indices (white lines and dots) derived by summing various normalized anomalies from different parts of the environment (coloured bars stacked above the abscissa are positive anomalies and those below are negative). The panels sum anomalies for the shallow, intermediate, and deep layers (from top to bottom). Anomalies for variables in parentheses are "reverse" colour-coded, because higher indices of these reflect colder conditions.